2-1-2012

Large strain flexural testing of thin composite laminates

Mikhail Grigoriev

Mikhail M Grigoriev
Candidate

Mechanical Engineering
Department

This thesis is approved, and it is acceptable in quality and form for publication:

Approved by the Thesis Committee:

Dr. Mahmoud Reda Taha , Chairperson

Dr. Thomas Murphey

Dr. Yu-Lin Shen

LARGE STRAIN FLEXURAL TESTING OF THIN COMPOSITE LAMINATES

by

MIKHAIL M GRIGORIEV

B.A., PHYSICS,
OCCIDENTAL COLLEGE, 2006

THESIS

Submitted in Partial Fulfillment of the
Requirements for the Degree of

Master of Science
Mechanical Engineering

The University of New Mexico
Albuquerque, New Mexico

December, 2011

Dedication

To my parents for all of their sacrifices.

Acknowledgments

I would like to thank my mentor, Dr. Thomas Murphey, for his guidance and support. I am honored to have worked for an engineer of Dr. Murphey's expertise. I also would like to thank my advisor, Dr. Mahmoud Reda Taha, for his belief and support.

This work was carried out in parallel to ongoing research at Air Force Research Laboratories – Space Vehicles Directorate. I would like to thank Dr. Brandon Arritt for supporting this project and the rest of the group for lending a hand. A special thanks to Gregory Sanford for his calm and collected approach to all the challenges we faced and conquered along the way.

Preface

During the course of this thesis (2010-2011) the following papers have been published or submitted for publication in reviewed proceedings or scholarly journals:

1) Murphey, T. W., Sanford, G. E., Grigoriev, M. M., "Nonlinear elastic constitutive modeling of large strains in carbon fiber composite flexures," 16th International Conference on Composite Structures, June 2011., Porto, Portugal.

2) Sanford, G. E., Ardelean, E. V., Murphey, T. W., and Grigoriev, M. M., "High strain test method for thin composite laminates," 16th International Conference on Composite Structures, June 2011., Porto, Portugal.

Large Strain Flexural Testing of Thin Composite Laminates

by

Mikhail M. Grigoriev

B.A., Physics, Occidental College, 2006

M. S., Mechanical Engineering, University of New Mexico, 2011

Abstract

Carbon fiber composites are of significant interest for use in deployable space structures. Elastically folded thin laminates can be utilized as hinge mechanisms in structural systems such as solar arrays, reflectors, and instrument booms, allowing for compact packaging during launch to orbit. While the initiative to utilize composite laminates in deployable structures has increased it also has faced difficulties in design and analysis of these poorly understood materials. Data from standardized ASTM test methods fails to characterize nonlinear constitutive behavior over the full large strain range common to deployable structures. Flexural behavior is characterized by the moment vs. curvature response therefore requiring a bending test. A special test fixture is developed to allow flexural testing of thin plates at large strains. Reaching large strains during the test provides an opportunity to investigate the large strain linear and nonlinear elastic constitutive behavior of glass and carbon fibers respectively.

A flexural test campaign was carried out for three unidirectional continuous fiber reinforced plastic materials in a large deformation four point bending fixture. Intermediate and high modulus PAN and S2 fibers were tested because they are commonly used in deployable structures. The fixture is designed to apply load, which through translation and rotation of wheeled carts, induces a pure moment in the sample.

We utilize a previously developed first order nonlinear empirical constitutive model to represent fiber axial tensile and compressive behavior and rule of mixtures with a linear matrix model for laminate behavior. We use algorithms for nonlinear curve fitting of moment-curvature response measured using the test fixture and fit for a nonlinear constitutive parameter and fiber volume fraction.

Using previously reported nonlinear tension parameter for IM7 fiber of 21.4 we estimated for the fibers' nonlinear compression parameter to be $\gamma_C = 20.7$. For test data of S2 fiberglass made by A.G.Y. and M55J carbon fiber made by Toray® the fit model did not differentiate between nonlinear constitutive parameter in tension or compression. Analysis of the experimental data returned a large nonlinear constitutive parameter of 97.6 for M55J fiber and a small nonlinear constitutive parameter of 6.7 for S2.

Contents

List of Figures

List of Tables

Chapter 1
Introduction

The objectives of this research were to measure and model the large strain or deformation bending properties of thin carbon and glass fiber composite plates used as structural hinge mechanisms. A large rotation flexure test fixture was developed utilizing four-point bending to allow specimen thickness as low as 50 μm to be tested in flexure. In addition, the data collected was fit to a previously established constitutive model for the non-linear behavior of carbon fibers. The unidirectional laminates tested were made of Hexcel® IM7 carbon fiber with Hexcel 8552 toughened epoxy resin, Toray® M55J carbon fiber with TenCate® RS-3 cyanate ester resin, and A.G.Y. S2 fiberglass with Patz Materials & Technologies PMT-F7 toughened epoxy resin. Traditional fabrication methods of thin laminates result in non-uniform fiber and resin distribution and wavy

surface geometry. A new method was developed to improve the geometry of the test samples.

1.1 Motivation and Background

The growing interest in composite materials is not limited to typical stiffness and strength per mass driven applications, but includes areas where traditional mechanisms can be replaced by large strain and high stiffness composite flexure hinges. It has been previously established that the tensile and compressive behavior of carbon fibers is nonlinear for strains greater than 1%. This behavior is typically not accounted for in the analysis of thick composite structures such as aircraft wings and rotors which are subjected to large deformations but relatively small strains. Deployable space structures, on the other hand, rely on parts made of thin laminates able to sustain strains on the order of 2% and for which nonlinear behavior is significant and cannot be ignored.

In deployable space structures, the traditional mechanical approach and the material deformation approach differ in the complexity of the design and cost. The sliding contact joints, utilized in mechanical approach, are necessary to render the structure in deployable configuration but increase complexity and cost of design/production. Such costs are eliminated in the material deformation approach where structural flexure joints are used to withstand large elastic strains first during packaging stage and later during the deployment process. In addition, the high modulus to density

ratio of carbon fiber composite decreases cost by reducing weight and the number of parts necessary for implementation. Structures benefiting from simple composite hinges can be anything from a phased array and linear antennas to solar sails and instrumentation support structures. The Air Force Research Laboratory has a number of structures under development which employ material deformation for deployment [1], [2].

The scope of this work is focused on measurement of the large strain constitutive behavior of thin composite laminates including carbon and glass fiber types. This thesis presents the procedures developed, as well as data analysis, for specimen manufacturing and testing. The test data is used to estimate nonlinear parameters to accurately model material behavior under large strain. The models and their statistical fit to the collected data will be discussed in greater detail.

The newly developed test fixture presents a unique opportunity to measure and simulate failure strain levels of various thin specimens. The fixture design allows in particular for a variation of specimen size and was built to test samples of dimensions used today in deployable structures to eliminate scaling issues. Many researchers have tested carbon and glass composites and observed large strains, but none have applied a pure moment to the range of specimen thickness considered here.

Developing and measuring composite response under pure bending is very challenging. This thesis provides the testing and analysis methods as well as other details to meet this challenge. The reported results provide new insight on the behavior of very thin composites under very large strains.

1.2 Thesis Outline

The thesis begins with a literature review (Chapter 2). The literature review conveys existing knowledge of various ways carbon and glass fibers have been tested to determine their constitutive behavior. Manufacturing standards for thin composite laminates are reviewed due to the importance of properly made laminates for testing. Finally, a brief history of the nonlinear constitutive model used here is presented with previously found nonlinear parameters and tests used to find them.

Chapter 3 introduces the new mechanical test fixture used to induce large strains in thin laminate specimens with pure moment. The geometric relationship is derived between the known dimensions of the fixture, specimen, and load, to determine the desired moment and curvature values. This chapter also goes into the details of manufacturing the specimens for testing from various types of fiber and matrix. The test procedure, data collection, and posttest analysis are also discussed. Explanation of the model fit through algorithms using mathematical software and source of error wrap up the chapter.

Chapter 4 presents the data from the flexure test and tabulates the analysis from fitting the models to the collected data. The first case study of IM7/8552 carbon fiber composite has a previously determined parameter thus allowing a complete nonlinear

model evaluation. Such data has not been collected for the rest of the composites and a different approach focusing on the signs of nonlinearity is presented and discussed.

Finally, chapter five provides a summary of the research findings regarding the use of the new fixture and its use to induce a pure moment to thin laminates in large flexural strains. We also discuss the reliability of the modeling approach and the future work required to better understand and model the behavior of composite flexures.

Chapter 2
Literature Review

2.1 Fiber Elastic Behavior

First reported by Curtis, Milne and Reynolds [3] Type I and Type II carbon fibers (heat treated at 2500^{o}C and 1500^{o}C respectively) show a linear increase in modulus with tensile stress. The authors related this phenomenon to a progressive axial alignment of crystallites. Numerous studies conducted since this observation have reported on the influence of microstructure on carbon fiber strength and modulus [4-7]. The crumpled graphite sheets which make up the fiber, shown in Figure 2-1, are the mechanism behind the fibers' nonlinear behavior. Under load, the graphite sheets first go through bending mechanisms as crumpled sheets straighten out, and then axial extension along straight graphite sheets.

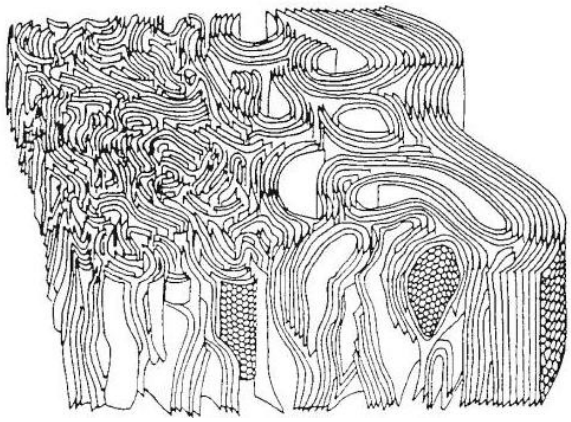

Figure 2-1: Rendering of a high-modulus graphite fiber microstructure [8]

Constitutive behavior nonlinearities have been observed and reported by Loidl et al. for both pitch and PAN carbon fiber composite laminates [9]. Jones and Johnson showed compression instabilities as fiber surface wrinkles and bumps which developed into local surface buckling [10]. Other researchers reported bulging and crystallite buckling [11], [12]. Unlike carbon fibers, glass fibers have not been reported to show nonlinearities in their constitutive behavior. Glass fibers are made of randomly array of silicone-dioxide and other molecules and do not go through bending mechanisms experienced by carbon fibers.

2.2 Fiber/Lamina Testing and Behavior

Studies of thin carbon composite laminates have shown higher compressive strengths [13] and tensile strengths [14] obtained from flexural testing compared with traditional tensile and compressive tests. Glass failure strains twice the common expectancy were observed in single fiber elastic loop test developed by Sinclair, who reported flexural strains as high as 5.6% in a very small volume of glass fiber [15]. Flexural strains of

approximately 3.2% were shown using the same method in carbon fibers by Jones and Johnson [10]. The elastic loop method used on a PAN based carbon fiber with tensile strains of 3% by Thorne achieved average flexural strains of 4.9% [16]. Thin composite laminates have also demonstrated similar compressive strain behavior as single fibers, laminates reaching failure strains of 2.5% [17]. Wisnom suggested total laminate thickness plays a major role in the ability of a thin coupon to reach high compressive strains. This was explained by the proximity of the fibers in tension that would provide some restraint to the compression fibers that prevents buckling [17].

2.3 Application of Thin Composite Flexures in Structures

There are a variety of applications for thin composite flexures in deployable space structures. Applications include solar arrays, reflectors, antennas, gravity gradient booms, and instrument booms. Self-Contained Linear Meter Class Deployable (SIMPLE) CubeSat boom, and a Triangular Rollable And Collapsible (TRAC) booms are just two examples of flexible composite structures developed by the Air Force Research Laboratories [2], [18-20]. In the SIMPLE boom, two pairs of carbon fiber tape springs were wrapped around a hub and deployed in opposite directions upon release as shown in Figure 2-2. The TRAC boom collapses from its stiff, straight, V-shape into a sliver that wraps around the body of the primary mechanism for stowage, as shown in Figure 2-3.

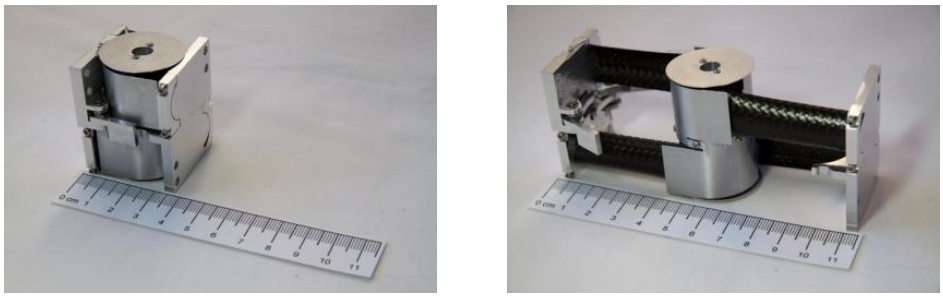

Figure 2-2: Thin composite laminate stowed and partially deployed

Figure 2-3: Partially rolled Triangular Rollable And Collapsible (TRAC) Boom

2.4 Flexural Testing of Thin Composite Plates

Composite materials are accepted in deployable structures even though their high strain levels are currently poorly understood making design and analysis of such structures difficult [21]. Current ASTM standards do not offer test methods outside traditional loading applications which can characterize the nonlinear constitutive behavior over the full strain range of deployable structures [21]. The ASTM standard D 3039/D 3039M is used for determining in-plane tensile properties of polymer matrix composites by measuring the response of a thick coupon subjected to a simple stress state over a large

area [22]. In this standard method, a coupon with a constant rectangular cross section is monotonically loaded in tension by a standard testing machine which holds the sample with grips. Ultimate tensile strain and modulus are determined through strain gauges adhered onto the test sample. The specimen length, width, and thickness are shaped as needed to contain a sufficient amount of fibers in the cross section to show a clear representation of the bulk material [22].

The ASTM D6272-02 standard for measuring flexural properties of reinforced plastics by four-point bending tests assumes a length of 50.8 mm for all samples less than 1.6 mm in thickness with a 25.4 mm gage length between supports. The specimen is be deflected until a fiber strain of 5% or rupture has occurred in the outer fibers [23]. The test can be performed with two types of loading cases, a load span of 1/2 or 1/3 of the length of the support span. The maximum stress occurs between the two load points between which the moment is also maximum and constant. The four-point bending tests for plastics, ASTM D6272-02, fail to properly test samples thinner than 1.5 mm within 5.0% strain limit due to limitations and restriction of the fixture. At maximum load and minimum support span a thin specimen would simply flex but not fail.

The ASTM D6272-02 standard appropriate for testing reinforced plastics is popular for testing reinforced carbon and glass composites. Jones has evaluated the four-point test and described it as inapplicable to multimodulus materials such as carbon fiber composites [24]. O'Brien et al. used the three and four-point bending tests not only to determine the strength of 24 and 36 ply unidirectional samples but also to characterize transverse tension life fatigue [25], [26]. Mujika used three and four-point bending test to derive the modulus of elasticity of carbon/epoxy samples [27]. Like O'Brien, the carbon

fiber samples Mujika used for testing were of standard thickness between 1.5 and 4 mm. The samples from the tests were at least one order of magnitude thicker than the samples discussed in this text. The standard ASTM test for flexural properties and others, such as the pinned-end buckling, demonstrated elevated flexural strains in composites, but failed to give accurate results for samples thinner than half a millimeter. Thus, a new testing method was deemed necessary. This test method was recently developed and used to derive flexural properties of thin composite laminates at AFRL laboratories [21].

2.5 Manufacturing practices for unidirectional, flat, composite coupons

Geometrically consistent parts are critical for accurate testing. In order to produce laminates with desired specifications a correct manufacturing process and method is important in composite manufacturing. Autoclave, oven, and hot pressing are some of the common processes for coupon manufacturing. The autoclave method relies on a pressure chamber heated in appropriate cycles, based on the manufactures' specifications of the matrix material in use, while controlling vacuum and/or pressure [28]. Manufacturers of matrix materials provide appropriate cure cycles for their product.

The variations in cure cycles stem from the type of matrix material in use with the fiber and the process used. The matrix materials are made for different purposes and vary in ingredients, mechanical properties, cost, and more. Cyanate Ester and epoxy resins are the two most common types of thermoset matrix systems used in the aerospace community [28], and were the two types of matrix systems used for two different carbon fibers evaluated in this text.

In composite manufacturing, a number of extra materials are commonly used as secondary or specialty materials for part production. Figure 2-4 demonstrates a typical autoclave lay up of a composite laminate surrounded by necessary secondary materials for production of a desired part. Peel ply, porous release film, bleeder plies, breather plies, all serve a distinct purpose in the composite part production. Volatiles are released as the matrix viscosity lowers with heat. With the help of breather plies, volatiles are sucked away by the vacuum created in the bag. Peel plies help the cured part to come off a caul plate with ease. Porous release films and bleeders help contain the extra matrix material squeezed out from under the vacuum or pressure. Resin dams keep the caul plates from moving and excess resin from escaping, while the vacuum bag surrounds the whole assembly and squeezes it tight to help get all of the air and volatiles out [28].

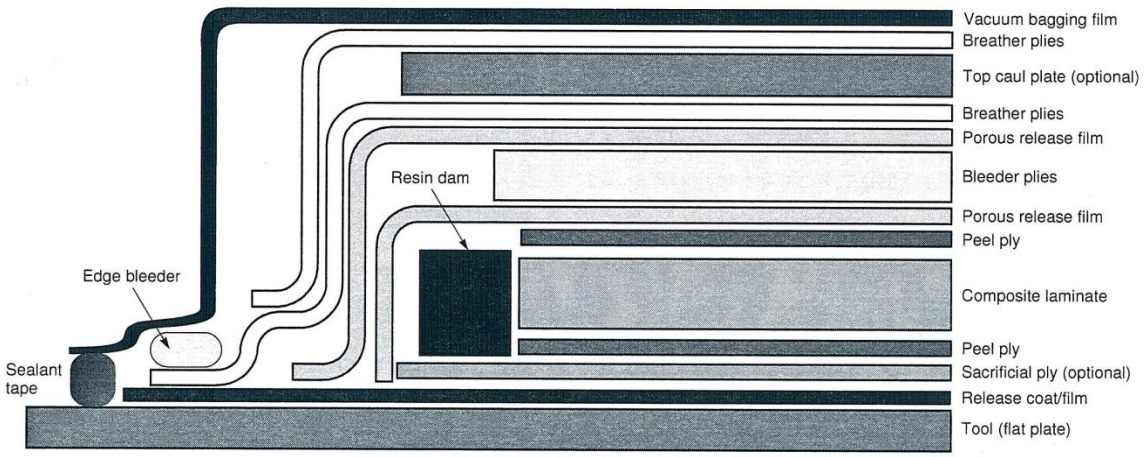

Figure 2-4: Typical layup configuration for a composite laminate autoclave cure [28]

High pressure autoclave cure leaves a surface imprint on the composite part even with a presence of a uniformly thick plastic peel ply. The surface pattern of the composite was determined by the layering of the specialty materials used in direct contact or close proximity. Most release films and bleeders are woven from nylon, fiberglass,

Teflon, and other polyester type materials. Topographical variations on the surface have driven some to polish the effected surfaces post cure. Polished surface in tension did not produce and in fact decreased fatigue life of a carbon and glass fiber composite [26] and overall strength measured by three and four-point bending tests [25]. Instead, a straight, non-polished surface with minimal amount of matrix pooling will increase reliability of results by cutting down variation in thickness across the gauge surface.

2.6 Modeling Nonlinear Behavior in Composite Materials

In several studies the axial nonlinear elastic constitutive behaviors of carbon fibers and carbon composites were represented using polynomial models. Ishikawa first introduced second order in modulus strain based models and Reder for stress based models [29], [30]. Murphey et al. rewrote the models to express the nonlinear parameters as non-dimensional and to multiply either strain or stress to the first power. The strain-based, second order form of Murphey et al. model is,

$$E_\varepsilon = E_o(1 + \gamma_1\varepsilon + \gamma_1\gamma_2\varepsilon^2) \quad \text{(Eq. 2-1)}$$

and the second order, stress-based form is,

$$E_\sigma = E_o(1 + a_1\frac{\sigma}{E_o} + a_1a_2\frac{\sigma^2}{E_o^2}) \quad \text{(Eq. 2-2)}$$

E_o characterizes initial modulus at zero load. γ and a are the non-dimensional parameters which characterize material nonlinearity described above [31]. The subscript on the non-dimensional parameters symbolizes the first or second order while the modulus E_o is a zeroth order parameter. Hughes introduced the first order strain model

based on simplifying Ishikawa's model [32] and the first order stress model was presented by van Dreumel and Kamp [33]. The models are written in first order form below,

$$E_\varepsilon = E_o(1 + \gamma_1 \varepsilon) \quad \text{(Eq.2-3)}$$

and

$$E_\sigma = E_o + a_1 \sigma \quad \text{(Eq.2-4)}$$

In general observations, modulus increases with strain or stress and the first order non-dimensional parameters are positive. The second order non-dimensional parameters are required only if modulus is observed to deviate from a linear increase with the applied stress or strain [31].

To model nonlinear behavior at the composite level, Murphey et al. used the nonlinear rule of mixtures to consider the fiber and matrix independently. Fiber level parameters were also derived from composite level parameters and the nonlinear parameters measured at the fiber level were found to be close to the ones measured in the composite level [31]. Murphey et al. tested their models using the raw data from study done by Welsh [34] of IM7 carbon fiber coupons impregnated with Cycom 997-2 epoxy in tension and compression. By assuming data from Welsh et al., to be an accurate representation of composite stress-strain behavior, manufacturer's reported modulus for epoxy, and laminate fiber volume fraction, Murphey et al. were able to capture the data well. The group found that standardized tests were appropriate for estimating first order nonlinear tensile parameters. Moreover, they concluded that the flexural test was

required to assess the models over large strain range due to high uncertainties in estimating first order nonlinear compressive parameter [31].

Many have investigated the flexural properties of carbon fiber laminate focusing on a variety of differences. The variation between some of the standard tests and test used here was that only a small volume of the material was under high stress. The strengthening of carbon fibers with a reduction in flexural coupon size was first accounted for by statistical strength theory based on a Weibull distribution [14], [35]. After observing large compressive strains in eccentrically loaded buckling test, Wisnom et al. concluded that the largest strains could not be fully explained by Weibull statistical distribution and were a result of through thickness strain gradients [13].

Murphey et al. used the results from a platen test method to further analyze thin laminates in flexure. The selected test method closely represented the operational state of material in a deployable structure but did not subject the flexure to pure moment. The platen test did not directly measure moment, curvature, nor did it apply pure moment to the sample. The specimens tested by Murphey et al. were also complicated by cross section inconsistencies.

Despite complications, the data analysis of the IM7 carbon fiber reinforced with Hexcel 8552 toughened resin allowed Murphey et al. to recommend an initial fiber modulus of 248.6 GPa and compressive and tensile nonlinear parameters of 29.6 and 21.4 respectively. Murphey et al. provided evidence for an accurate fit of a first order model with three parameters which characterize full strain range behavior of the tested carbon fiber. The work further concluded the parameters in question can be properly estimated from standardized axial tests and reliably extrapolated to the larger tensile strains

observed in flexures. The same could not be said for compressive parameters which require a larger strain test to for nonlinear parameter estimation than the current standard test provide.

Chapter 3
Fabrication and Experimental Methods

Introduction

This chapter describes the materials, sample fabrication, experimental test set up and procedure. The chapter also discusses the new testing techniques developed for measuring flexural strains in thin composite coupons. The materials chosen for this experiment represent a variety of fibers used by the aerospace community. The different resin systems, which fibers come pre-impregnated, also fit in the general use category of toughened epoxies and cyanate esters. Although manufactured by different companies, the resin systems stem from a very similar design, performance, and identical curing techniques. Flexural behavior is characterized by the moment vs. curvature response of a flexure requiring a bending test. The flexure test set up, based on a four-point bending test, and induces a pure moment in the gage section while reaching large rotation. The moment and curvature are calculated by measuring load and displacement during the test. Designed by Emil Ardelean of AFRL, a patent application has been submitted based on

the fixtures novel abilities. Figure 3-1 demonstrates the test set up by capturing the fixture pre, mid, and end of test in parts b, a, and c respectively.

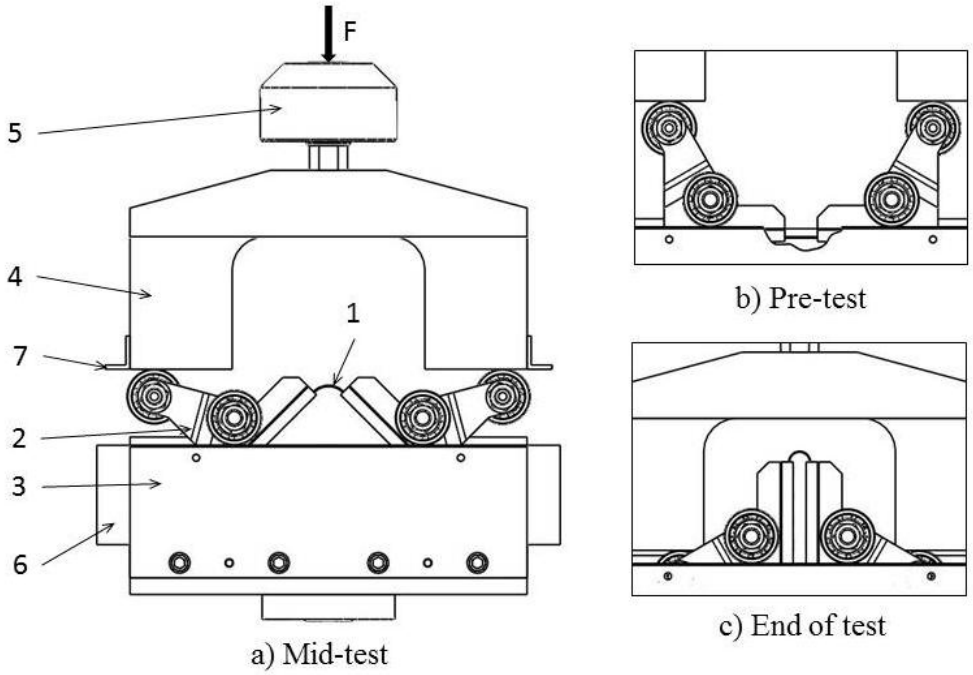

Figure 3-1: a) Schematic of the improved, pure-moment test fixture during test; 1 – coupon, 2 – carts, 3 – tracks, 4 – crosshead, 5 – force sensor, 6 – laser displacement sensors, 7 – laser displacement sensor target; b) starting position; c) largest specimen deformation: 180^{o} arc

3.1 Mechanics of the Flexure Test

Moment and curvature are calculated from the geometry of the fixture, measurements of the crosshead displacement, and applied axial load throughout the test. Point O is the midpoint of the coupons' gage section between the two carts shown in Figure 3-2. When load F is applied to the top bearings, the moment (M_o) at point O is:

$$M_O = \frac{F}{2}(l + x) - \frac{F}{2}x \qquad \text{(Eq.3-1)}$$

which simplifies to,

$$M_O = \frac{F}{2} l \tag{Eq.3-2}$$

As the crosshead applies load, the carts will begin to rotate to create pure moment described by Eq.3-2 in the coupon gage section. By knowing the resting vertical height between the two bearings h_o, the change in the crosshead displacement was measured using the laser displacement sensors.

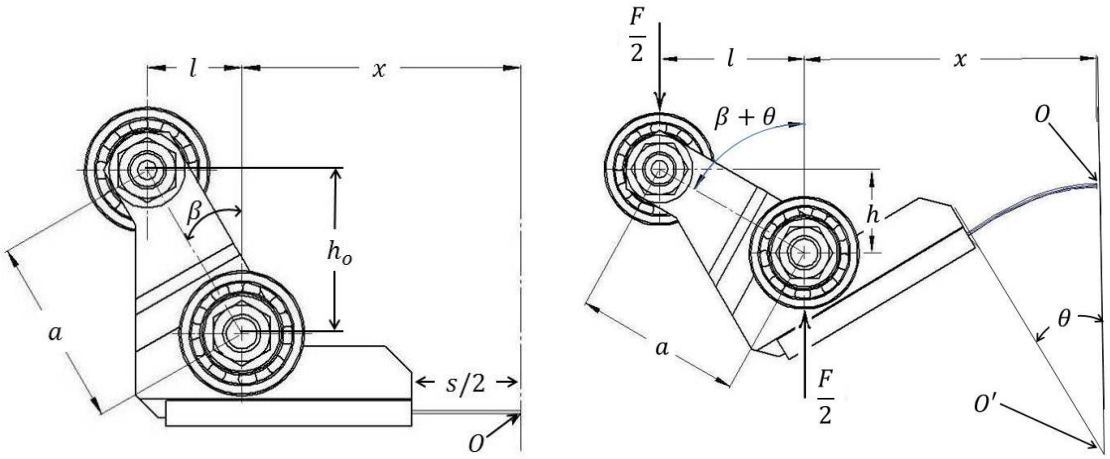

Figure 3-2: Free body diagram of a resting and partially rotated left cart

From the geometry seen above in the free body diagram of the cart,

$$l = \sqrt{a^2 - h^2} \tag{Eq.3-3}$$

The result for l from Eq.3-3 was substituted into Eq.3-2 and the moment is

$$M_o = \frac{F}{2}\sqrt{a^2 - h^2} \tag{Eq.3-4}$$

The length of the gage section is s, which is twice the length identified on the left side of Figure 3-2. The definition of curvature is change in angle per arc length:

$$K = \frac{\alpha}{s} \tag{Eq.3-5}$$

where $\alpha = 2\theta$ in our case. Figure 3-3 is a close up image of a laminate in bending between two carts. Distance s is physically set and measured prior to the test, α is

calculated from crosshead displacement using trigonometric relations from Figure 3-2 to find θ:

$$\theta = \cos^{-1}\left(\frac{h}{a}\right) - \beta \quad \text{(Eq.3-6)}$$

Substituting Eq.3-6 into Eq.3-5, we find curvature from directly measured quantities and known relations so that,

$$K = \frac{2}{s}(\cos^{-1}\left(\frac{h}{a}\right) - \beta) \quad \text{(Eq.3-7)}$$

Assuming a linear material model, the neutral axis is coincident with the plate mid-plane, regardless of curvature. Here, a nonlinear model was assumed, and the neutral axis shifts towards the stiffer tensile side of the coupon as curvature increases. This shift will be calculated in section 3.9. However, for test sizing purposes, the assumption of a linear model can assist in determining an appropriate initial separation.

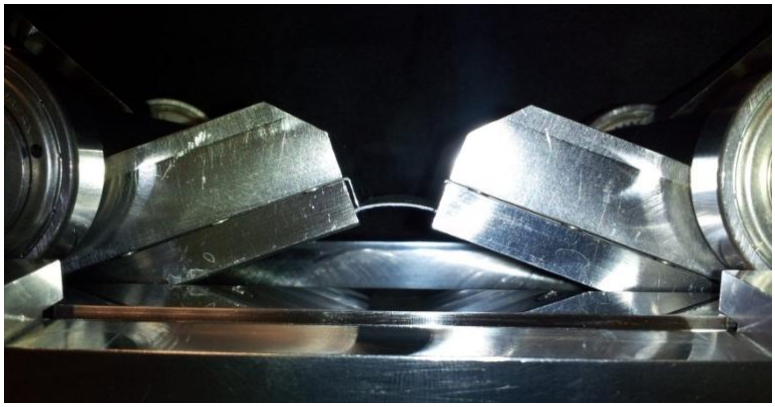

Figure 3-3: Carbon fiber laminate specimen in pure bending

The maximum strain occurred at the surface, contained half the thickness t away from the neutral axis, and calculated,

$$\varepsilon_{max} = \frac{t}{2}K \quad \text{(Eq.3-8)}$$

Using experience from prior testing the distance between the two carts was preset based on the thickness of the sample. This way maximum strain in the new test fixture was

reached at $\alpha = 180^o$ and catastrophic failure was guaranteed. Eq.3-5 can be evaluated at $\alpha = \pi$ to give:

$$s = \frac{\alpha}{K} = \frac{\pi}{K} \quad \text{(Eq.3-9)}$$

By substituting the solution for *K* from Eq.3-8 into Eq.3-9, the initial cart spacing *s* can be found for a maximum strain value expected in the specimen:

$$s = \frac{\pi t}{2\varepsilon_{max}} \quad \text{(Eq.3-14)}$$

Using Eq.3-14 we can easily find top end thickness limitations for materials tested in this thesis. Based on the manufacturer specified strain level and geometrical limit for gage length of 4.046 cm, we find a IM7 carbon fiber laminate of up to 553.0 μm thick can be tested in full fixture motion of 180°. S2 glass fiber, which fails at approximately 4.5% strain, has a maximum thickness capacity of 1382.5 μm for a full fixture motion test of 180°. The full fixture motion is not necessary but is preferable.

3.2 Materials

Several materials were selected for this experiment including IM7/8552, M55J/RS-3, and S2/PMT-F7. IM7 is intermediate modulus carbon fiber with high strain to failure and stiffness properties. M55J carbon fiber also has twice the modulus, is much stiffer, and has a lower strain to failure properties then IM7. Unlike IM7, M55J has not been extensively tested and thus is of high interest to us. S2 fiberglass is used as a reference

material because it has much higher strain to failure properties than carbon fiber, lower modulus, and has not been found to behave as a nonlinear material.

IM7 was pre-impregnated with 175^{o}C cure toughened epoxy resins and M55J was pre-impregnated with a blend of cyanate ester. S2 is a glass fiber selected for its high flexural strains as previously discussed in Chapter 2. To increase reliability in parts production, the matrix materials for the three types of fibers were chosen on the basis of their similar 175^{o}C curing cycle recipe. Table 3-1 outlines some of the fiber and matrix properties available from the manufactures of the specified materials.

Table 3-1: Properties of fiber and composite laminates

	Tensile Strength GPa	Tensile Modulus GPa	Tensile Strain	Flexural Strength GPa	Flexural Modulus GPa
Hexcel IM7 carbon fiber	5.6675	275.79	1.8%		
Hexcel 8552 epoxy resin	0.121	4.67			
Toray M55J carbon fiber	4.0196	539.2	0.8%		
TenCate RS-3 cyanate ester	0.080	2.97	4.9%	0.1269	3.32
AGY S2 glass fiber	4.8898	86.9	2.0%		
Patz Materials PMT-F7 epoxy resin		3.496			

3.3 Pre-Fabrication

After conducting a micrograph study, described in section 3.6, of samples with various thicknesses used in the platen test by Sanford et al, a pattern was found in the cross sections of the samples which increased analysis difficulty [36]. Observations of the continuous wavelike deformation in the cross section of samples, as shown in Figure

3-4, spurred development of a new curing method somewhat different from the accepted manufacturing process for thin composite plates.

The old manufacturing process for composite laminates utilized a number of woven materials and plastic films to surround the pre-impregnated carbon fiber during the curing process. These extra layers of materials were used to pull air and volatile gasses trapped in carbon fiber prepreg sheets while resin flowed throughout to fill in the voids. The processed carbon fiber panel takes the shape of a sandwich which contains a prepreg in the middle, perforated Teflon (AirTech® TFP234) on either side, a layer of fine weave peel ply used as a bleeder (AirTech® Release Ply B), and squeezed between machine ground steel caul plates covered in a thin plastic film which acts as a release ply (AirTech® A4000R).

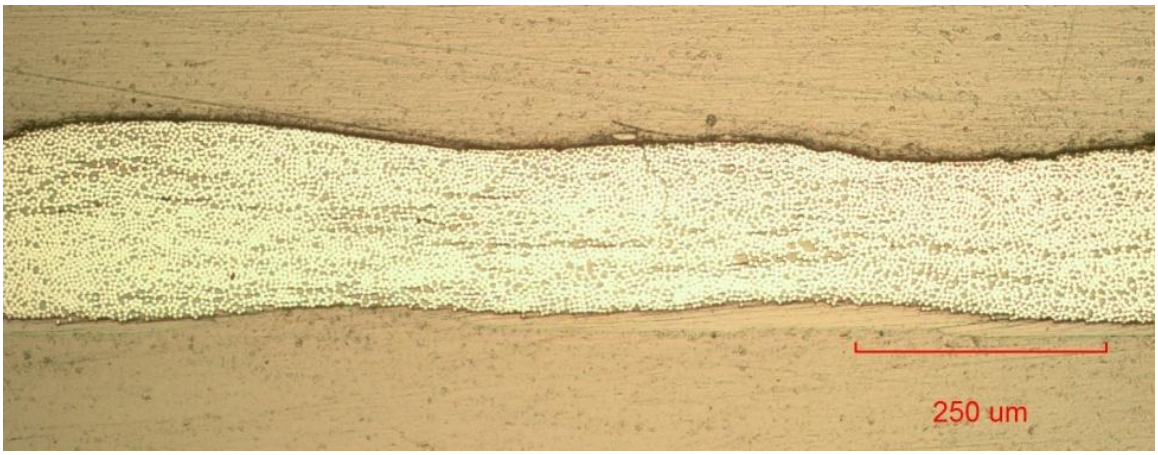

Figure 3-4: IM7/8552 Two ply unidirectional cross section x10 magnification using old style of lay-up showing significant waiving and excess resin pools on the surface

This process has proven to produce quality parts thicker than half a millimeter with a small variation in surface topography. In the current study, the sample thickness under investigation ranged between 50 µm and 500 µm. Topographical variations of the surface play a major role in the analysis, thus requiring a higher tolerance level for

thickness precession. The 550 kPa pressure in the curing cycle transfers the weave pattern of breathers and bleeders into the part, displacing some of the carbon fibers and creating an uneven distribution of resin on both the top and bottom surface of the panels. By removing materials which help the excess gasses escape, we were able to avoid the weave imprint in the samples as shown in Figure 3-5.

A curing study was carried out to discover the most effective method for creating smooth surfaced laminates with less than 10% thickness variation throughout the plate. A variety of layup techniques were tested. Covering caul plates in thin plastic release films seemed most suitable but proved to trap even the smallest amounts of volatiles leaving surface depressions. AirTech® recommended its own breathable membrane, Dahtlexx, for its smooth surface. Unfortunately, the membrane had sponge-like properties and failed to keep a constant thickness throughout the composite laminate.

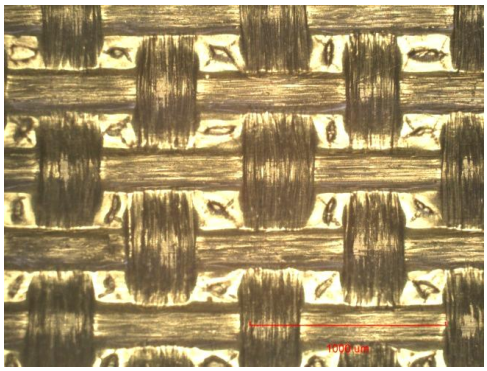

Figure 3-5: Surface of a cured old style IM7/8552 plate x5 magnification

Recent advances in pre-impregnated materials have minimized volatiles trapped in the processing and released during curing. Figure 3-6 shows a cross section of a tested material used in the curing method selected to make all of the laminates for the flexure fixture testing. A simple coat of a release agent on the caul plates and positive stops

shims on the perimeter were enough to produce excellent parts, described in detail in the following section.

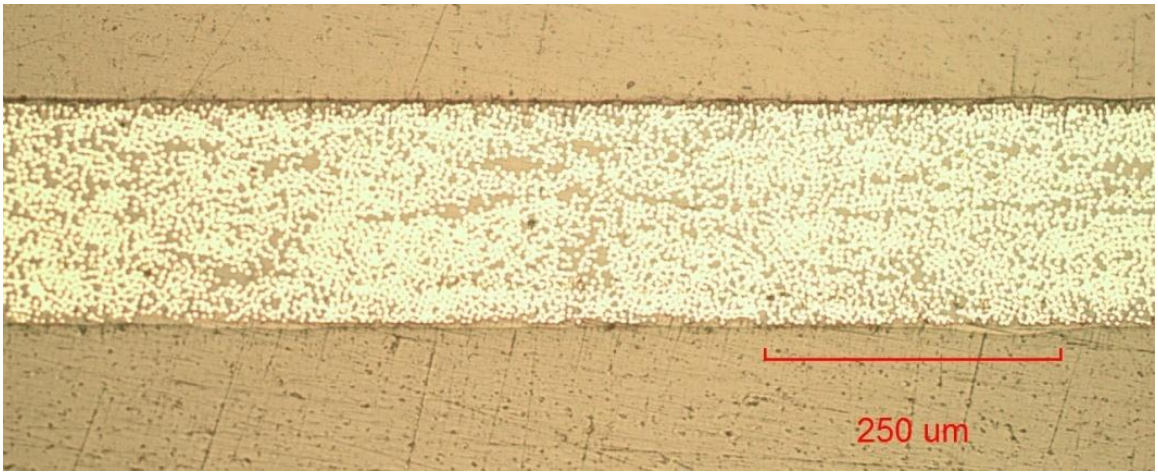

Figure 3-6: IM7/8552 cross section of new 2 ply unidirectional x10 magnification using of

Sealed and mold release treated precision ground caul plates left a noticeable imprint mirroring the machine ground faces in the laminate surfaces as shown in Figure 3-7. A close examination of the topographical variations showed an increase in flattens and the cross section of the lamina to be within accepted limits.

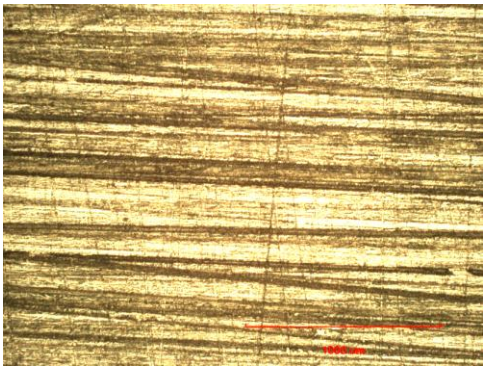

Figure 3-7: Surface of a cured new style IM7/8552 plate x5 magnification

3.4 Laminate Fabrication

To begin the process, the parts which come in contact with composite material, primarily caul plates and shim stock used for positive stops, were cleaned using Isopropyl and treated with liquid form of Frekote® B-15. B-15 is a sealant agent for metals which coats the surface and prevents resin from penetrating small cracks and bonding to the metal. Prior to each cure, the caul plates or other metal surfaces coming into contact with resin need to be cleaned with Isopropyl and additionally wiped down with a mold release agent. Frekote® 700-NC was used in our process and pairs well with the B-15 sealer. Pre-impregnated material was kept in -18.0^{o}C freezer to preserve shelf life and was allowed to warm up to room temperature prior to handling.

The prepreg arrives on rolls and must be cut down to appropriate length and desired angle to the fiber direction. There is no standard for the size of laminates. At AFRL/RVSV, 305x305 mm caul plates are typically used to create same size parts. Due to an over squeeze of resin from applied pressure during the cure cycle, positive stops were required to keep the desired fiber ratio to resin volume. A fiber volume fraction of 0.6 is an industry standard to which we tried to adhere. A 12.5 mm border was left around the perimeter for positive stops making the square parts 280x280 mm. After warming up to room temperature, the prepreg was cut into appropriate size squares using the Gerber® mechanical cutting table shown in Figure 3-8.

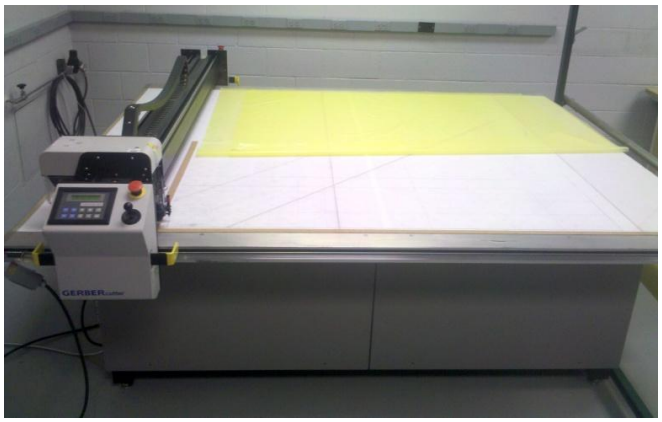

Figure 3-8: Gerber® mechanical cutting table

A single ply of IM7/8552 with a 32% Fiber Areal Weight (FAW) varies 10% in thickness as a result of resin loss in the cure process. Without positive stops to prevent the pressure from squeezing substantial amounts of resin out, the final laminates may be 80% fiber by volume.

Final laminate thickness depends on the number of prepreg plies it contains and the thickness of the positive stops. Two panels of the same thickness were required to produce enough coupons for testing. Four sets of coupons, with different thicknesses or ply numbers, were required for each material. Testing three materials with four variations in thickness, a total of 24 laminates, were produced for this experiment. IM7 panels were made of two, three, four, and five plies per panel with an average cured thickness per ply of 100 µm. Thicker materials, such as S2 glass, had one ply in its thinnest panel, 120 µm per ply, and went up to four plies in its thickest laminate. M55J contains three plies in its thinnest panel, 40 µm per ply, and due to the high modulus of the material only two more thicknesses were produced – six and nine plies. The final panel count was 22 as shown in Table 3-2.

During the buildup of panels a number of standard methods must be followed. First the panels were aligned using a right angle fixture, shown in Figure 3-9, and stacked no more than three plies at a time. De-bulking three plies at a time prior to further build up is required in manufacturing out of carbon fiber prepreg.

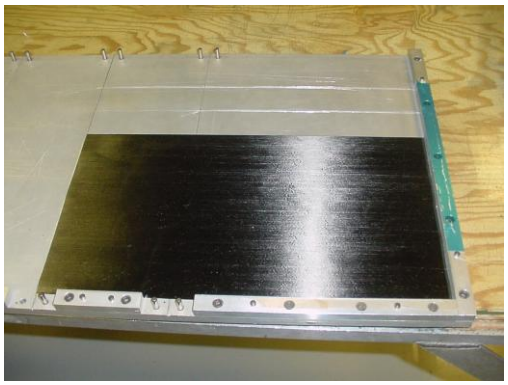

Figure 3-9: Alignment fixture for panel lay up

Table 3-2: Matrix for laminate plate production

Material	# of plies	Average thickness (μm)	# of laminate plates/coupons made for testing
IM7/8552	2	200	2/8
	3	300	2/8
	4	400	2/8
	5	500	2/8
M55J/RS-3	3	120	2/6
	6	240	2/6
	9	360	2/8
S2/PMT-F7	1	115	2/8
	2	230	2/8
	3	345	2/8
	4	460	2/8

All panels were subsequently de-bulked to decrease gaseous voids introduced by stacking material together using a heated vacuum table as shown in Figure 3-10 at a temperature of 45-50^{o}C. A smooth glass surface and an envelope bag are also appropriate for de-bulking process. The paper carrier film was removed from the prepreg after two plies were aligned and stuck together unless the material needed to de-bulk first.

Figure 3-10: Heated vacuum table

Panels were marked with the fiber/resin type, thickness, and a line parallel to the fiber direction with an appropriate color sharpie for the material (silver on carbon panels and black on glass fiber panels). Not all panels were cured at one time. The extras were properly labeled on the paper backing of each panel and on each moisture resistant bag. Extra panels wait for their turn in the freezer to preserve freshness of the matrix material while the others make their way to the autoclave.

A standard curing thickness of 100 μm per ply of IM7/8552 with a 32% resin was held by building up a shim stock dam around the prepared panel. A shim stock tolerance of 6.5 μm per ply was kept at all times. De-bulked prepreg and shims were arranged on a bottom caul plate, as shown in Figure 3-11. The shims were taped to the bottom caul plate to prevent them from moving during the next step.

Figure 3-11: S2 fiber glass panel surrounded with shims on a caul plate

Suctions cups with handles were used to carefully lower top caul plate on the pre-impregnated panel surrounded with shim stock. A square perimeter dam, made out of blue Aircast 3700 rubber by AirTech®, was fitted around the top caul plate, and a J-type thermocouple was taped against the rubber dam and bottom caul plate shown in Figure 3-12. Thermocouple wire was imbedded into the sealant tape, one wire at a time, and covered with more sealant tape to prevent air leakage. The assembly was completely covered by a thick blanket-like material (AirTech® N-10) to help guide air out of the encapsulated part as shown in Figure 3-13.

Figure 3-12: Rubber dam around a caul plate with a thermocouple

A vacuum port was installed by cutting a small hole in a semi-stretchy bagging material (AirTech® SL700), fitting the foot of the port from the inside of the bag, and tightly screwing a locking ring onto the foot from the outside of the bag. The vacuum bag seals the blanketed caul plates together with the help of vacuum tape (General Seal 43MR) stuck to the perimeter edge of the bottom caul plate. Vacuum was pulled through the port to check for ability of the bag to hold vacuum shown in Figure 3-14.

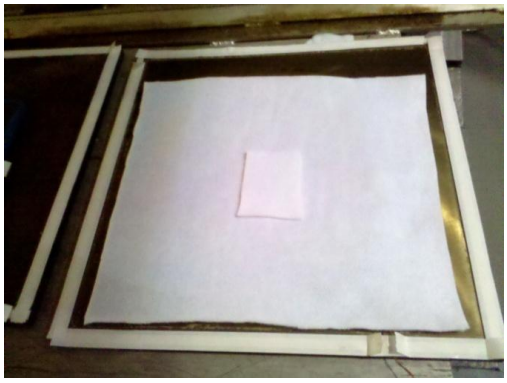

Figure 3-13: N-10 Placed on top of caul plate

Figure 3-14: Vacuum drawn on sealed panels prior to cure

A vacuum rate loss of no more than 2 kPa per minute was acceptable and was tested for upon immediate completion of the vacuum bag. Some leaks were easily dealt with by applying more pressure on the bag over the sealant tape area and smoothing out any existing folds in the bagging material. Forcing small amounts of sealant tape into

areas with leaks was also appropriate. If air continues to leak above approved rate and no specific source can be identified and fixed, the bag must be replaced with a new one. Vacuum hose and thermocouple were connected to/from the bagged part inside the autoclave to appropriate ports shown in Figure 3-15. The 175^{o}C cure cycle was selected from pre-programmed cycles and executed over an approximately eight hour period to allow for two main steps. Step one was an hour hold at 100^{o}C, and step two was a three hour hold at 175^{o}C. The first hold provides enough time for the resin to turn viscous and envelop the fibers while letting excess gasses and some resin to escape into the N-10. The three hour hold at higher temperatures fully cured the resin. Table 3-3 presents all the steps required for the curing process used in fabrication of composite laminates. The matrix materials used in making samples for testing described in this text go through an exothermic stage. At temperatures around 150^{o}C, the resin kicks and follows its designed cure kinetics until it fully solidifies around the fibers.

Table 3-3: Autoclave curing cycle segments

Segment #	Action	Temperature	Vacuum	Pressure
1	Heat to 100°C	rate @ ~ 5°C/minute	-100 kPa	0
2	Hold at 100°C for 1 hour	105°C > T > 95°C	< -80 kPa	0
3	Heat to 175°C	rate @ ~ 5°C/minute	0	55.2 kPa
4	Hold at 175°C for 3 hour	180°C > T > 170°C	0	> 48.5 kPa
5	Cool down to 35°C	rate @ ~ 4°C/minute	0	0

The curing cycle was programmed to run off the temperature value measured by thermocouples embedded into the composites for accurate measurement. Cured laminates were gently removed from the autoclave following completion and were freed

of any resin flash shown in Figure 3-16 that may have built up on the edges during the process.

Figure 3-15: Panels ready for cure in autoclave

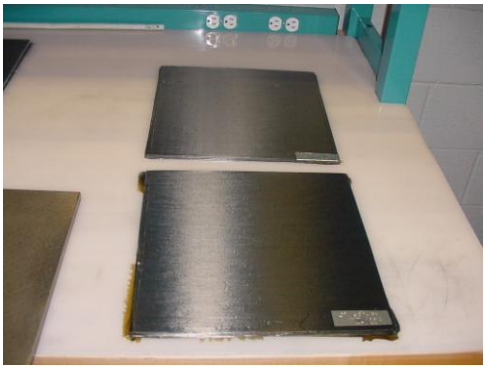

Figure 3-16: Cured carbon fiber plates with resin flash on the sides

Following the curing cycle, the panels were visually inspected for voids and overall thickness using a micrometer. Panels outside the 10% thickness variation limit were excluded. To prepare samples to fit the specifications of the bending fixtures, the cured plates were affixed to square board made out of G-10 and submitted to the machine shop for cutting. Spray-77 adhesive, manufactured by 3M®, was used to bind the panels

to the G-10 backing boards. The strong adhesive was ideal to keep the pieces from falling apart during machining yet easily diluted and wiped clean with Acetone. The samples were cut to 50x150 mm coupons with the help of the line on the panel indicating direction of the fiber. The long side of the coupon was machined parallel to the fiber direction.

Once cut into appropriate size, the samples were carefully marked with appropriate information using a laser engraver and de-bonded from the stiff backing plate. Due to possibility of the coupon critically failing in the gage section and falling apart, the coupons were marked twice at opposite ends for future reference. Excess adhesive was gently cleaned off using scotch bright in an acetone bath.

Prior to testing, each sample was carefully measured with a micrometer to determine an average thickness across the center line and by calipers to measure the width. The thickness measurement was used as an initial reference for basic data plotting. The true sample thickness was measured post-test when they were micro-graphed using a calibrated microscope and appropriate computer software. To keep track the samples were assigned a batch number and a sample number marked on the samples in addition to the already existing material and cure information. The measurements of each sample were cross referenced with the batch and sample numbers for ease of identifying all of the dates/time, cure cycles, material/roll/batch numbers, and other information that may become important.

3.5 Test Fixture Setup

Once the test samples were ready the test fixture can be carefully taken out of its storage container always using non-powder gloves while handling it. In order to capture the best results possible any and all contamination of contact surfaces was avoided. A sketch of the alignment fixture, the carts, and the alignment clamps is show in Figure 3-17. The carts were released from the alignment clamp and clamping plates were removed from both carts as shown in Figure 3-18. With a lint free rag, all of the carts surfaces need to be wiped down with isopropyl. The rag was moistened first, so no direct isopropyl was spilled onto the cart or into the bearings. The clamping plates and bolts were thoroughly cleaned and the surfaces were examined for any excess materials which would prevent the samples from being tightly secured. The top surfaces of the alignment fixture and clamp were also cleaned prior to returning the carts and lightly securing them in it.

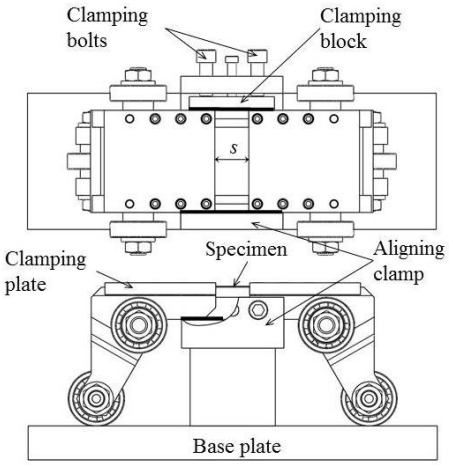

Figure 3-17: Alignment fixture

Figure 3-18: Carts in the alignment fixture with one of the sample covers removed

After cleaning the carts, a light abrasive pad was used with isopropyl to gently work the surfaces of the load head and rails. Four ball bearings were exposed while carts were upside-down in the alignment assembly, and in order to achieve the smoothest and cleanest plane possible, they receive the same scotch bright treatment. The other two bearings were cleaned once the cart assembly, with the test sample, was transferred to the load frame but prior to the alignment clamp removal. Tools such as adjustable parallels and calipers, which come into contact with either carts or load frame, were also cleaned to ensure dirt and oil free environment. The clamping plates may be placed back onto the secured carts if the samples, which were going to be tested, do not have strain gages. The samples were simply slid in-between the holders and the carts from either left or right side before the holders were secured to the carts with bolts. If samples did have strain gages on them, the samples were placed onto the aligned carts and covered by the clamping plates while keeping the strain gage leads to the side.

The carts were designed to handle samples up to two inches in width. Samples that were slightly less than two inches wide must be aligned to either side of the clamping plate simply by pushing the sample to meet the edge, and samples that were substantially smaller need to be placed in the middle using calipers to get correct alignment. Adjusting

the distance between carts was another step required prior to securing the clamping plates to the carts. The distance between carts depends on the thickness of the sample and the approximate strain levels which were desired at $\alpha = \pi$, described in section 3.1, to which the carts will be driven/rotated to using the load head.

Adjustable parallels or precision gage blocks may be used to accurately set predetermined distance; the carts were tightly squeezed together keeping the gage tool between them and the bolts were lightly tighten shown in Figure 3-19. The samples cover was secured with six bolts each preferable tightening the bolts in a star pattern. A set of digital calipers were used to double check the distance after removing the gage tool. Once the sample was secured between the carts the alignment clamp can be tighten to fully contain the carts from any possible movement during transfer to the load frame.

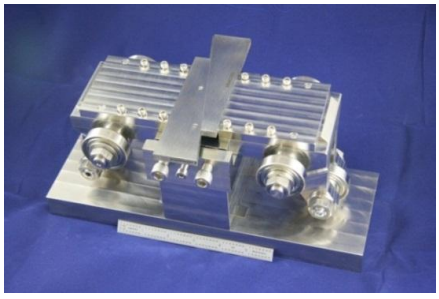

Figure 3-19: Carts in the alignment fixture with adjustable parallels setting the gage length

The load head and the bottom rails were designed for compatibility with an MTS load frame. Both the rails and the load head were carefully assembled in the load frame with an appropriate sized load cell. To properly align and affix all the necessary parts, the load head was driven into a channel at the bottom of the rail assembly shown in Figure 3-20 a. All the necessary bolts and nuts were tightened and the load head was driven up to check for physical alignment using a calibrated Pro 360 digital protractor.

The protractor was placed along the rails and across to verify a 0.0^{o} tilt. The same was done to the load head.

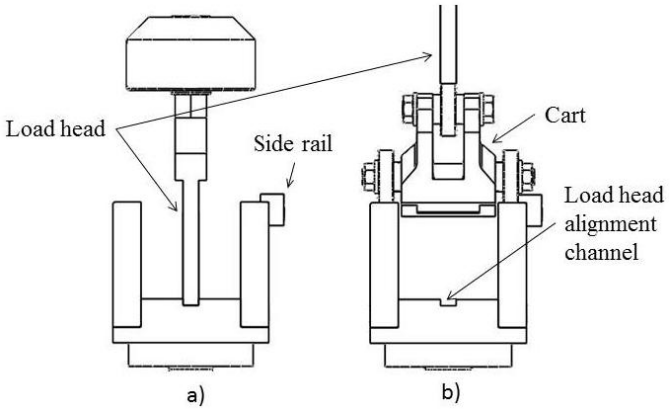

Figure 3-20: a) Alignment of top and bottom assemblies; b) alignment of carts on tracks

Prior to the transfer of the assembly to the load frame the MTS equipment has to be checked and laser displacement sensors calibrated. Two precision two inch blocks were set onto the rails, and the load head was driven down to just touch the blocks as shown in Figure 3-21. Each block was carefully tested by moving it left or right to make sure the load head was in contact with it. If either block moved freely the load head may have needed to be readjusted or even shimmed until a desired level of horizontal precision was reached.

Once the load head was in contact with the precision block the laser displacement sensor Mid Span was reset. The laser displacement has a range of 100 mm in order to fully capture all of the fixture movement which starts at 96.993 mm above the rails. Setting the laser mid-range at 50.8 mm above the rails allowed the operator to capture all of the movement. At midpoint the laser signal read 50.0 mm, since that midpoint was 50.8 mm above the rails there were only 46.193 mm left between the midpoint and the top of the initial flexure fixture position. Subtracting the midpoint offset and adding the

result to the midpoint of laser signal produces the exact reading according to the laser displacement sensors at which to begin the test: 96.193 mm. Upon completing the calibration the rails and load head should be cleaned with a lint free rag damped with isopropyl.

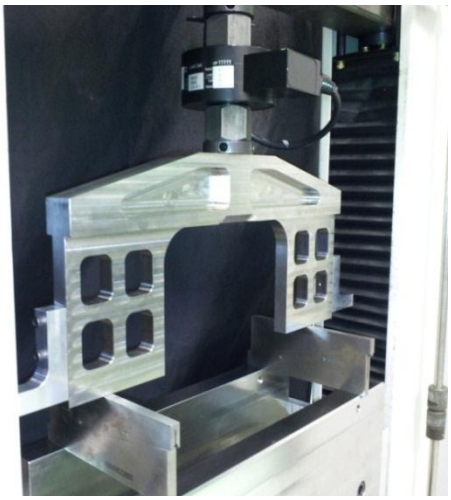

Figure 3-21: Calibration of laser displacement sensor with precision blocks between test surfaces

When the load head and rails were aligned and cleaned test could begin. The four exposed ball bearings were cleaned once more, and the aligned fixture with the sample was carefully transferred into the load frame. If there were wires running to the strain gages in the sample, the leads shall be kept from snagging prior to the whole assembly being set onto the rails.

The first step after the carts were placed into the load frame was to clean the surfaces of the two bearings which were previously inaccessible due to their role in properly aligning the fixture shown in Figure 3-17. The assembly should be placed tight against the side rail which was attached by two bolts to the rails to ensure the carts and the load head were perfectly parallel to each other. The whole assembly was centered in

the load frame and the load head was driven down to just touch the upper bearings for equipment functionality check.

A load of approximately one tenth of a Newton must be placed on the clamped carts in order to make sure that the load head was in proper contact with the top bearings. The recording equipment must be running in test mode while load and laser distance should read the current applied load and the initial laser displacement distance of approximately 96.193 mm.

If the setup was found to be functioning properly, the load head could be repositioned a few millimeters above the upper bearings and the alignment clamp may be removed. With ample pressure applied to the alignment clamp by the operator in order to keep the whole fixture from moving, the clamp bolts were loosened and the clamp was carefully removed. The carts proper position shall be checked with the side rail by firmly pulling them against it. The bolts on the side rail were then loosened, and the bar was pulled back to prevent the ball bearings from causing unnecessary friction through contact. The carts were gently moved side-to-side to check for any irregularities and distribute internal lubrication evenly around the bearing. The load head was repositioned back as close to 96.193 mm as possible without going under.

To induce pure moment on the gage sample, the fixture relied on six Nachi Quest shielded ball bearings shown in Figure 3-22. The Nachi ball bearings were standard electric motor bearings with a C-3 radial clearance. Initially, six ABEC-7 precision unshielded bearings were used to test capabilities of the flexure fixture. Soon after losing one very expensive ABEC-7 bearing to an unclean environment, a comparison of the two types of bearing was made by simulated conditions of the flexure test. The less

expensive Nachi bearing earned its spot when no difference in performance was found between the two. The ball bearings have been identified as a potential source of error further discussed later in this chapter.

Figure 3-22: Nachi Quest 6004 ZZENR shielded bearing [37]

3.6 Data Collection

An MTS load frame with an electromechanical screw-drive with a maximum capacity of 4,448 N was used for the new test fixture. Test set up in the load frame is shown in Figure 3-23. Cart separation distance *s*, specimen thickness *t*, and width *w* were recorded prior to the test. Displacement was measured with two Micro-Epsilon laser displacement sensors and load was measured with a 100 N or a 1000 N capacity load cell. The data was recorder in a three column text format partially shown for a 5-Ply IM7/8552 sample in Table 3-4.

Table 3-4: Typical data collected during specimen testing

Voltage - Laser Left (mm)	Voltage - Laser Right (mm)	Voltage - Load (N)
96.166953	96.188014	0.868472
96.095975	96.116999	1.287332
96.018544	96.062123	1.545092
95.928209	95.945917	1.835073
95.850778	95.832938	2.253933
95.763669	95.70382	2.479473

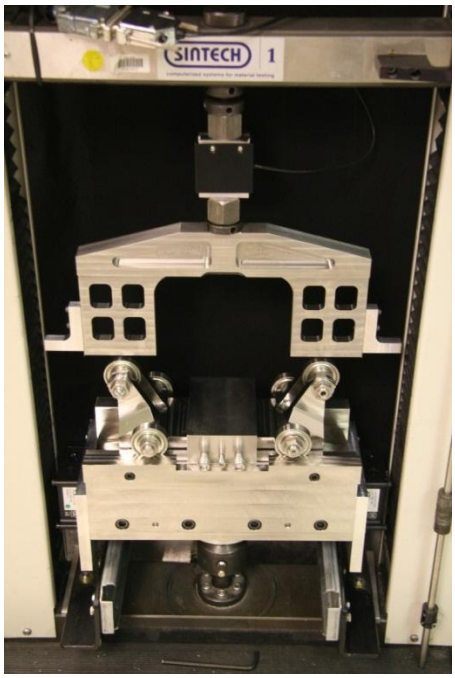

Figure 3-23: MTS load frame with the new test fixture

The average of the left and right laser displacement sensors was subtracted from the initial laser contact height (96.193 mm) and set equal to change in h. Knowing h_o and corresponding load from the third column of the data we calculated the moment at each reading described by Eq.3-4 and curvature described by Eq.3-7. Moment per width and tangent bending stiffness per width were plotted vs. Curvature as shown in Figure

3-24. Data from each sample was reformatted into a Comma Separated Value (CSV) file and processed by the code further explained in section 3.9.

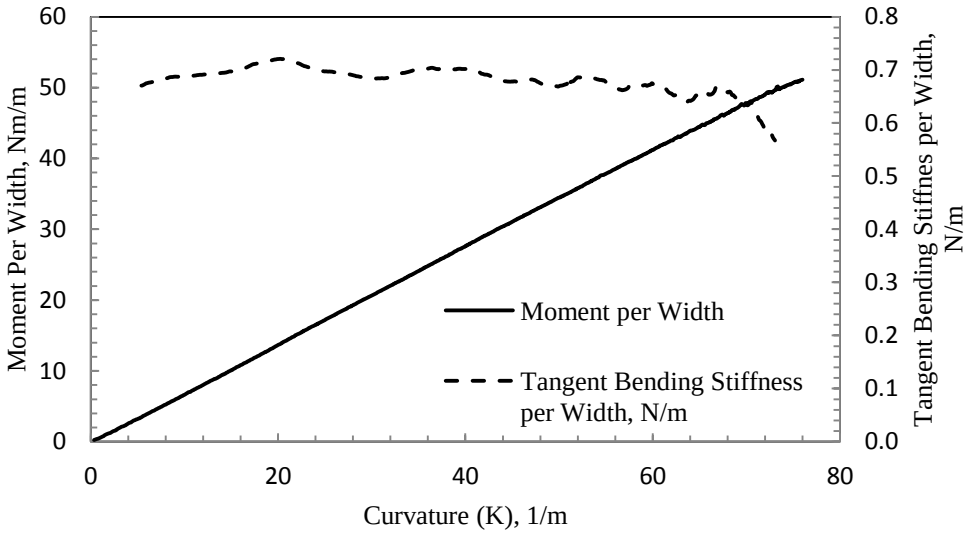

Figure 3-24: Moment and Tangent Bending Stiffness vs. Curvature plot for IM7/855-2 sample

3.7 Fixture Validation

Prior to collecting data from composite laminates, the fixture underwent a validation test using high carbon 1095 hardened and tempered spring steel. The objective of the test was to compare the modulus found from the flexure test with a modulus obtained from a tensile test in order to validate the new fixture. One standard tensile test was carried out using a tensile load frame and a center-mounted strain gage. Due to a well-documented material behavior there was no need to carry out more tests. Linear fit, between 1,000 με and 6,000 με, of the tensile stress vs. strain test data revealed a modulus of 204.2 GPa, shown in Figure 3-25.

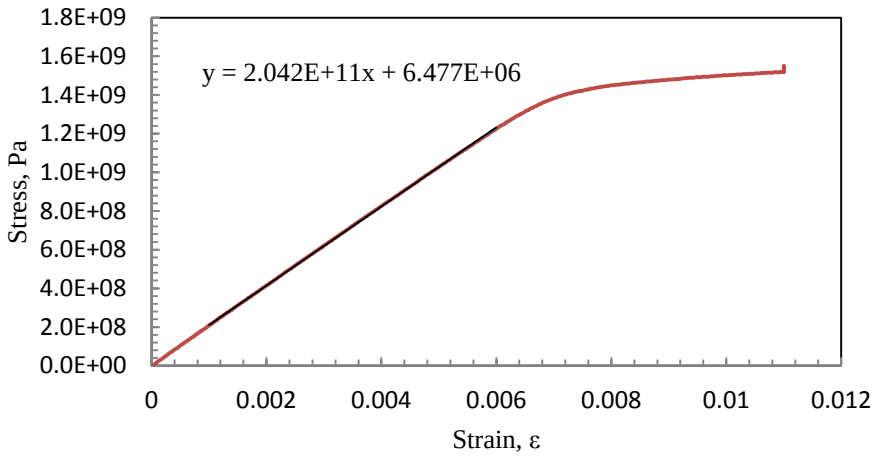

Figure 3-25: Spring steel tensile test

The moment vs. curvature data for three steel specimens is shown in Figure 3-26. Three tests gave a good statistical representation according to Student-t Distribution [38]. The flexural moduli for the three samples were found to be 205.1 GPa, 205.3 GPa, and 202.8 GPa. The modulus average for the three flexure tests is 204.4 GPa and is within 0.1% of the modulus found in the tensile test. The acute precision of the fixture allowed us to continue its use to test laminates.

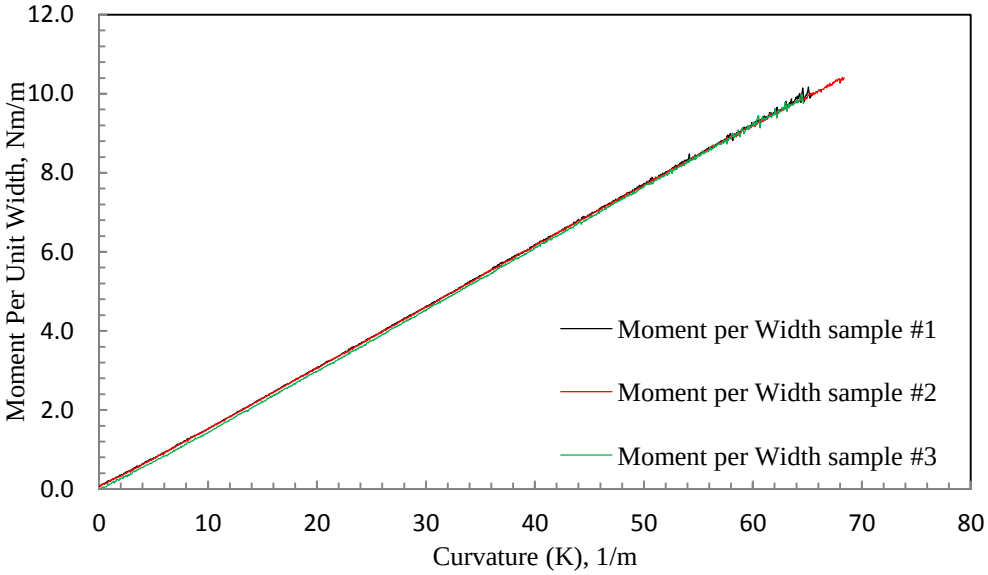

Figure 3-26: Spring steel flexure tests Moment vs. Curvature plot

3.8 Micrographing

To fully model unidirectional behavior of carbon fiber under large bending strains an understanding of consistent fiber/resin distribution and exact thickness is required. A small 25x15 mm square was cut out from each of the tested flexure coupons for micrograph study. In the study the cross section of the coupon was reviewed and measured under a microscope for variation of normal fiber/matrix distribution and precise thickness.

Prior to cutting the small squares out of the sample, the square dimensions, as well as indications which side was closest to the failure line and the surface side which was in tensions during the experiment were all marked. Out of five laminate variations, a sample from each tested flexure coupon was taken. Squares were appropriately marked as described above and divided into batches varying by number of plies in the laminates which they came from.

Samples with same ply number were placed into thin plastic stands to keep the samples upright and put into round cups with removable bottom which have been treated with Buehler #20-8185-002 release agent. Buehler® EpoThin quick setting epoxy and hardener were premixed in accordance to its directions, outgassed, and poured over the squares. The squares were then placed into a small vacuum chamber and left to further outgas for 15 minutes after which the cups were carefully removed from the vacuum chamber and left to harden for at least one hour.

The hardened cylinders were removed from plastic cups by pealing the bottom and applying pressure to the tapered side of the cylinder. Using a diamond blade a small sliver was cut off the cylinder using the Buehler® Isomet Low Speed Saw in order to

expose the cross sections of each square shown in Figure 3-27. An abundance of Buehler® Isocut fluid was required to keep the blade running smooth and straight at all times. A small weight can be added to the lever in which the cylinder sample sits as is cut by the blade in order to decrease the cutting time.

Figure 3-27: Buehler(R) Isomet Low Speed Saw

Once cut, the samples go through seven stages of material removal in order to polish the cross section to a mirror shine. The first two stages were 200 and 1200 grit resin bonded diamond grinding disk used with water on the polishing wheel for approximately two minutes each. The following stages require the use of Buehler® Ultrapad on the polishing wheel using 9, 6, and 1 micron diamond slurry to slowly decrease the size of the scratches on the cylindrical surface; each step requires its own Ultrapad and a sonic bath to remove large particulates prior to stepping down to smaller particulates. The slurry should be cut with Buehler Metadi fluid from time to time to keep the pad moist. Each step varies in time, the operator must constantly look at the sample surface and adjust the sample to make sure the material was removed evenly until no scratches were seen at x100 resolution.

Following the diamond slurry steps, a mixture of 0.3 µm and 0.05 µm Micropolish was made with distilled water. The operator should use the microscope for assistance to know when to move on from one mixture to the next and when to stop all together. The result of the process should reveal perfectly round cross sections of carbon fiber imbedded into resin as shown in Figure 3-28.

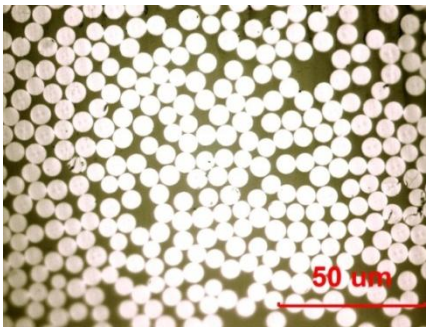

Figure 3-28: 2-Ply IM7/8552 x100 magnification post polishing

With the help of Nikon Eclipse LV150, we were able to look at the samples with a 5, 10, 20, 50, and 100 times magnification. Nikon digital built-in camera and Lumenera® software captured the work progress at each stage of the micrographing procedure, and most importantly, to record the thickness of each coupon tested using the fixture. The software was calibrated using a Graticules scale of 100 x 0.01 = 1mm at each of the magnification levels. A UV Fused Silica Ronchi Slide with 200 lines/mm from Edmund Optics was used to check the calibration to within 0.1%. The data was tabulated in the following Chapter.

3.9 Data Fitting

Once the sample thickness data was available from micrographing, the data fitting began. In order to process the data a previously written Worlfam® Mathematica notebook for

platen test was modified for use here. The code relies on a first order fiber strain nonlinear constitutive model with individual parameters for tension and compression. Axial nonlinearity in carbon fiber composites is primarily a consequence of fiber properties and therefore convenient to consider fiber and matrix independently. Matrix constitutive behavior is considered to be linear. Nonlinear rule of mixtures is used to find composite tangent modulus:

$$E_{c,rm} = E_o V_f + E_m(1 - V_f) \quad \text{(Eq.3-16)}$$

where V_f is the fiber volume fraction and E_m is the linear matrix modulus. Properties of fiber and matrix were discussed in Chapter 2.

The code computation is based on the following principals previously introduced in Chapter 2. First the nonlinear constitutive models were defined for stress and strain. Fiber strain constitutive model functions in tension and compression are defined from Eq.2.3:

$$E_T(\varepsilon) = E_o(1 + \gamma_T \varepsilon) \quad \varepsilon \geq 0 \quad \text{(Eq.3-17)}$$

$$E_C(\varepsilon) = E_o(1 + \gamma_C \varepsilon) \quad \varepsilon < 0 \quad \text{(Eq.3-18)}$$

where E_o is the fiber level modulus. Fiber stress is modeled for tension and compression in terms of strain by:

$$\sigma_T(\varepsilon) = \int_0^{\varepsilon} E_T(\varepsilon) d\varepsilon \quad \varepsilon \geq 0 \quad \text{(Eq.3-19)}$$

$$\sigma_C(\varepsilon) = \int_{-\varepsilon}^{0} E_C(\varepsilon) d\varepsilon \quad \varepsilon < 0 \quad \text{(Eq.3-20)}$$

Assuming no in plane load in accordance with test fixture design applying a pure moment to test sample, the in plane force integral was set to zero and solved symbolically in order to find the neutral axis (y_{na}),

$$N = \int_{-t/2}^{t/2} \sigma(\varepsilon)\, dy = 0 \tag{Eq.3-21}$$

where *t* is the thickness of the specimen, and strain is defined by:

$$\varepsilon = K(y - y_{na}) \tag{Eq.3-22}$$

where y is the location of the neutral axis under no load, or half the thickness. The Piecewise function in Mathematica was used to combine the independent tension and compression behaviors in Eq.3-20 & Eq.3-21 into a continuous function. Knowing the location of the neutral axis, we use our knowledge of the loads and moments required to produce a mid-plane deformation in any particular problem. The moment integral per width through the stress resultant is:

$$M_{per\,w} = \int_{-\frac{t}{2}}^{\frac{t}{2}} \sigma\,(y) dy \tag{Eq.3-23}$$

By fitting the test results for M and K as well as previously defined nonlinear tension parameter to the symbolically solved Eq.3-23 using the NonlinearModelFit function we get estimates and their statistics for V_F (fiber volume) and γ_C (nonlinear compression parameter) the parameters we were after. The NonlinearModelFit function uses one of six algorithms to return the best fitted results. Those algorithms are "Gradient", "Conjugate Gradient", "Levenberg Marquardt", "Newton", "Quasi Newton", and "NMinimize". The default algorithm selection was set to automatic for the software to choose the one which returns a model with a best fit accuracy. This process was

designed for a fiber such as IM7 which we know to be nonlinear and have a good approximation for γ_T.

S2 glass fiber does not exhibit nonlinear behavior as discussed in chapter 2. In order to verify that the previously written notebook in Mathematica was adjusted once more. The change in the notebook allows us to eliminate the nonlinear tension parameter γ_T and using the same model fitting function as before to solve for V_F and simply γ - the same nonlinear parameter in tension and compression. If the tested specimen displayed nonlinear behavior the model would return a positive fit for γ, but if the behavior is linear γ would equal to zero.

21.4 is used for the tension nonlinear parameter in IM7 model fitting. At this time we do not have a nonlinear tensile parameter for M55J or data from which a nonlinear tension parameter can be extracted. The M55J test data is subjected through the same model fitting process as the S2 fiber glass to capture one nonlinear parameter for both tension and compression at this time. Again, if laminate was to have nonlinear characteristics, the code would return a value other than zero for the γ parameter.

3.10 Error Analysis

The result obtained using the new fixture does come with a small error. Friction between contact points, inside the ball bearings, load cell, and laser displacement sensor accuracies were of primary concern. The rolling friction coefficient between the bearing and polished steel surfaces of the crosshead and the fixture was between 0.0002 and 0.0004 [33] and was deemed insignificant in our calculations [40]. The laser displacement sensors accuracy, according to the manufacturer, was within 0.03% at full

range of the device and decreased with range. By calculating a mean of the two laser displacement measurements the uncertainty was lessened and was considered unsubstantial.

The accuracy of the 100 N load cell, used for all of the testing except the IM7/855-2 5-Ply samples, was within 0.1% at 5% load and slightly increased with load. The large 1000 N load cell used in testing of 5-Ply specimens had the accuracy of approximately 0.3% at 25 N and decreased with additional compression load. All of the calibration reports for load cells and tools requiring calibration and used to complete this thesis can be found in Appendix A.

The load uncertainty was mitigated through standard laboratory practices of matching the load cell capacity to the loads applied during the test. Friction inside the ball bearings, between the shield and the ball bearings, was considered to be the most significant source of error and was analyzed further.

The 6004 ZZ deep groove bearings made by Nachi are double shielded with snap ring in order to provide superior protection from contamination such as particles from shattered test samples, dust, and more. These bearings are standard electric motor type with C-3 radial clearance. A low speed comparison experiment was set up between the Nachi shielded and the non-shielded ball bearings with ABEC-7 precision. The test identified no difference between two bearings in the amount of torque required to initiate bearing rotation while under loads similar to the loads expected in the test fixture.

Assuming a constant friction resistance, a free body diagram (FBD) can be drawn to include bearing rotation friction forces. The FBD of the test fixture was broken into three bodies: the ball bearing in contact with rails, the carts without ball bearings, and the

gage part of the sample. The three FBDs were used to show transition of frictional force from the bearings to the coefficient of moment induced in the specimen gage section. The FBD and lengthy equations are omitted here for briefness.

Another reason to omit full bearing friction model description is due to a rather complicating ball bearing movement during the test. In accordance with design, during initial application of load all six ball bearings horizontally move away from the center point *O* discussed in section six of chapter three. The lower four ball bearing reverse their horizontal movement when $\theta = 26^{o} \pm 0.5^{o}$ with the variation dependent on the distance *s* set between the carts. The upper bearings continue to move out until θ reaches 60^{o} at which point their horizontal direction is reversed. The three stages of movement present different challenges and allow for simplifications which were briefly explained here to omit the extended geometrical explanation.

The bearing friction effect on applied moment was initially large in comparison with applied force, but quickly dissipates as the load increases and was less than 2% at $\theta = 10^{o}$. The friction moment effect in Figure 3-29 shows the plotting of the friction moment contribution to the applied moment. The slight nonlinear inclination from straight line at the beginning of the validation data shown in Figure 3-26, is also a good example of small friction interaction.

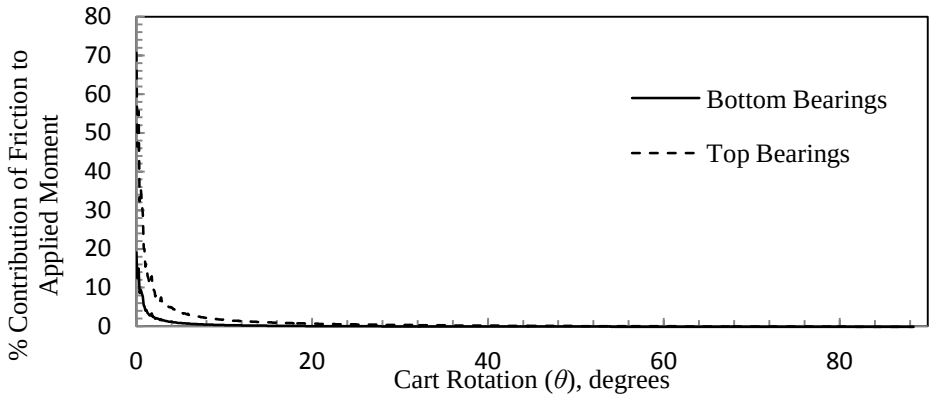

Figure 3-29: Bearing friction effect on applied moment

In some instances, the data fit model of the nonlinear parameter returned a large error coefficient. Assuming the cause of error was friction in the bearings, a small fraction of initial data was left out of the modeling. The error was dramatically reduced through this practice. By leaving a small initial data section from the fit in we were able to fit the model to experimental data with much higher precision. To ensure the legitimacy of leaving a fraction of the data from data fitting, a study was carried out to vary the amount of data left off and then fit to the model. In this study, the error first decreased and then increased after reaching a certain point in the collected data for each test. It was determined reasonable to leave off a small initial fraction of the data to increase the reliability of the model fit. This was deemed a necessary step in instances where full data fit returned a large error due to noise in the data.

Chapter 4
Results and Discussion

Introduction

The moment vs. curvature test data for all specimens are shown below in Figure 4-2 through Figure 4-4, grouped by fiber type. Only three plies of S2/PMT-F7 were tested due to higher than expected strains and limitations of the test fixture. The gage distance s between two carts for one ply of S2/PMT-F7 had to be 4 mm in order to reach 5% strain at α, but the minimum working distance s of the fixture is 6.5 mm. Testing the one ply samples below failure is unreasonable for our purpose and was not carried out.

The failure of carbon fiber laminates was catastrophic in all cases. Coupons failed along the grip where stress concentration is most likely to be present. In case of pure moment and absence of stress concentration points the coupon should fail in the middle of the gage section but this was not the case. Flexing the coupon around the edge of a stainless steel grip mechanism induced a premature failure at the load transition/concentration spot rather than in a desired area of the laminate which was the center of the gage section.

Fiberglass coupons did not fail catastrophically but also failed at the grips as shown in Figure 4-2. Because the coupons did not fail completely, they had to be cut in half in order to extract a sample from each for micrographing. Magnification of the failed region revealed delamination between the failed outer ply and the intact interior plies. According to observation, delamination occurred post outer ply failure while the coupon was still under load in flexure.

A substantial amount of fibers in compression were sheared across by the edge of the test fixture at which point the load application was discontinued by the operator. The specimen continued to handle the applied load without further shearing. This behavior indicates that the maximum strain range of the material was not reached.

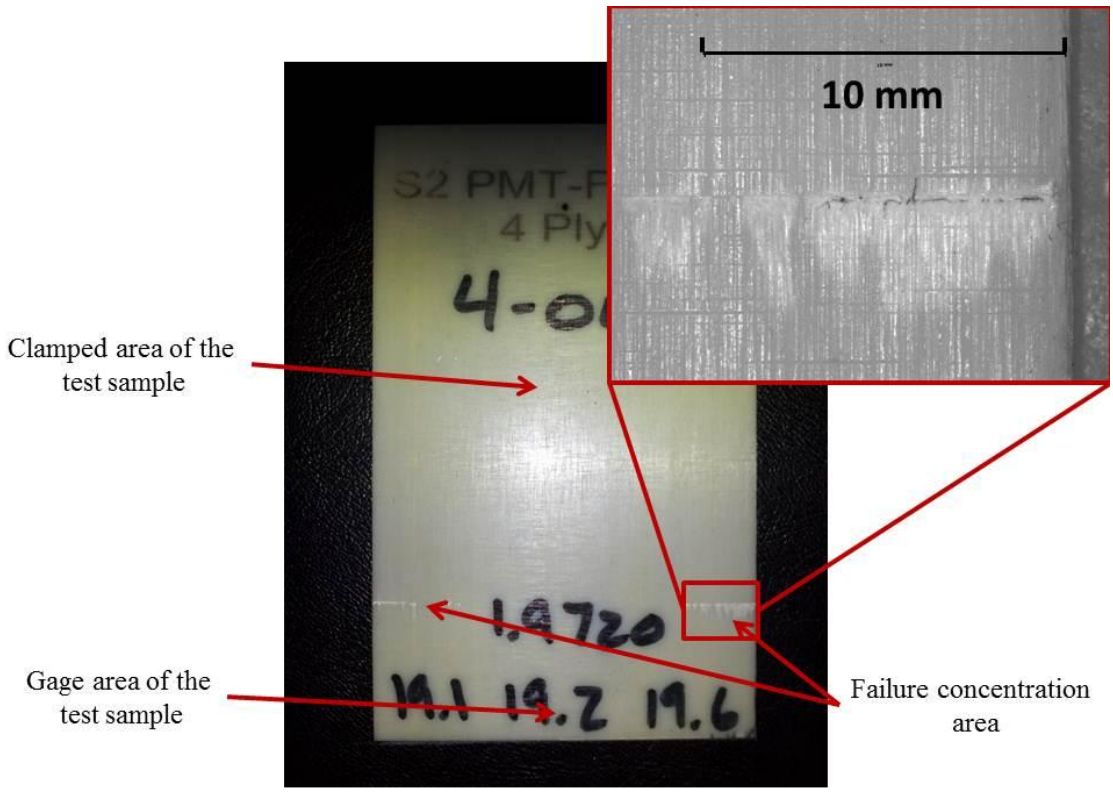

Figure 4-1: Half of a S2/PMT-F7 failed 4-ply coupon

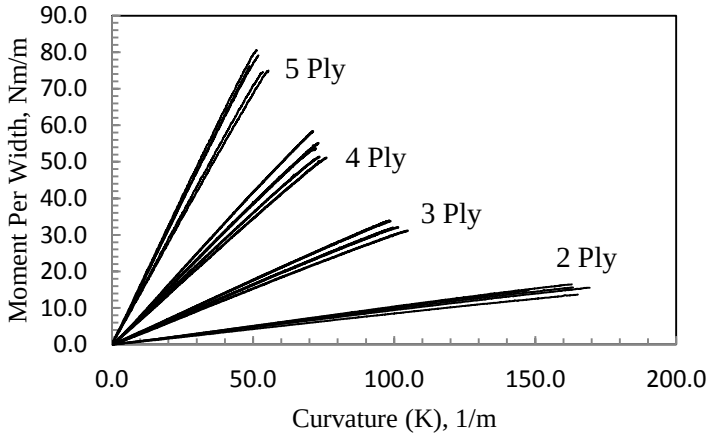

Figure 4-2: Test failure load as a function of thickness for IM7/855-2 specimens

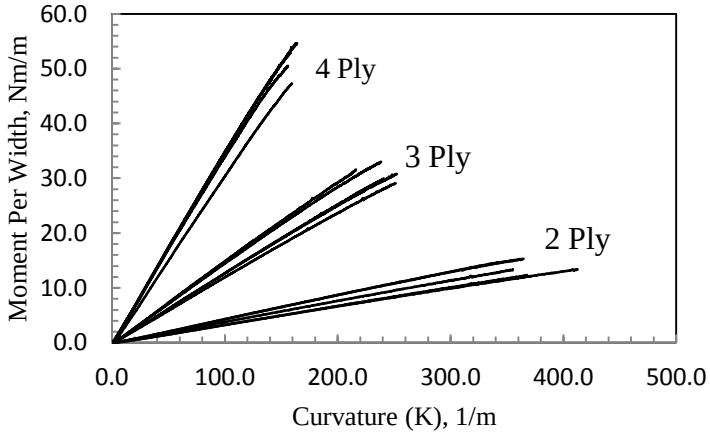

Figure 4-3: Test failure load as a function of thickness for S2/PMT-F7 specimens

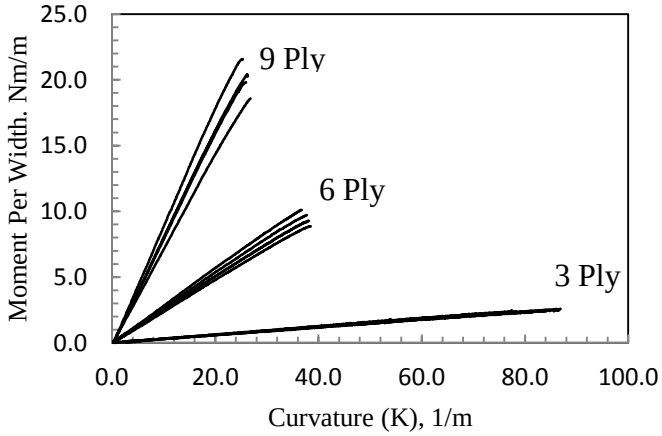

Figure 4-4: Test failure load as a function of thickness for M55J/RS-3 specimens

The cross sectional micrographs of every variety of lamina and thickness tested are shown below. The straight surfaces and minimal pooling of resin were desired and are apparent in the images. After examining the images closely, we can see thin lines of matrix material separating the plies in the IM7/8552 micrographs. The ply separation was less visible in M55J/RS-3 micrographs and was indistinguishable in the S2/PMT-F7 samples.

The three micrographs images at 100 times magnification of the three different laminates show distinctions in size, type, and volume fraction of the fiber. Both IM7 and M55J are PAN-derived fibers and almost perfectly circular [28]. According to Figure 4-8 c, the M55J fiber is shaped more like a kidney bean then a perfect circle. The effect of shape variation on the fiber properties is unknown. The S2 fiber nominal filament diameter is 9 µm according to the manufacturer. As shown in Figure 4-8 b, the fiber diameter varies from 7 µm to 10 µm.

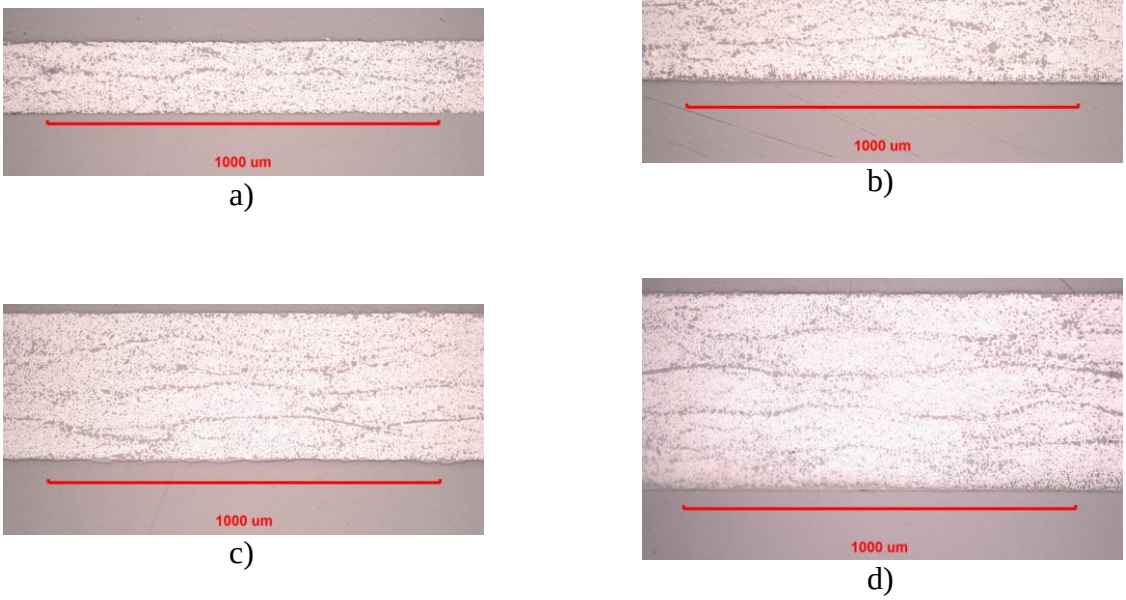

a) b) c) d)

Figure 4-5: Micrograph of IM7/8552 laminates: a) 2 Ply; b) 3 Ply; c) 4 Ply; d) 5 Ply.

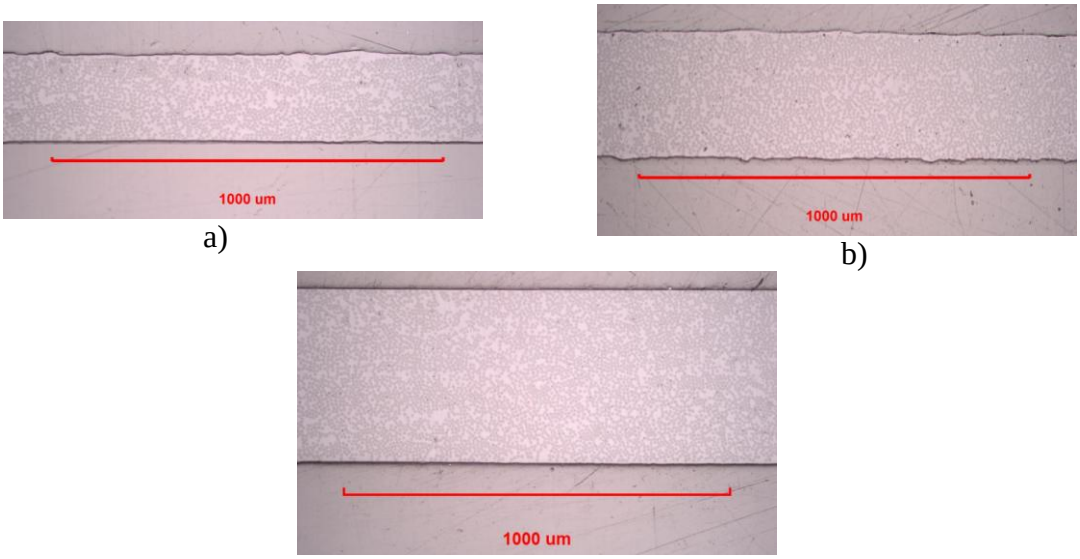

a) b) c)

Figure 4-6: Micrograph of S2/PMT-F7 laminates: a) 2 Ply; b) 3 Ply; c) 4 Ply.

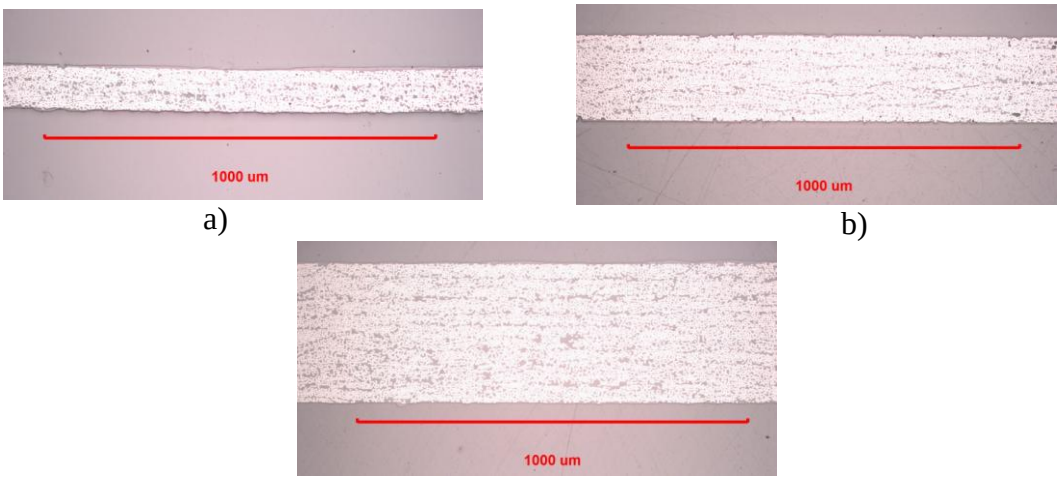

a) b) c)

Figure 4-7: Micrographs of M55J/RS-3 laminates: a) 3 Ply; b) 6 Ply; c) 9 Ply.

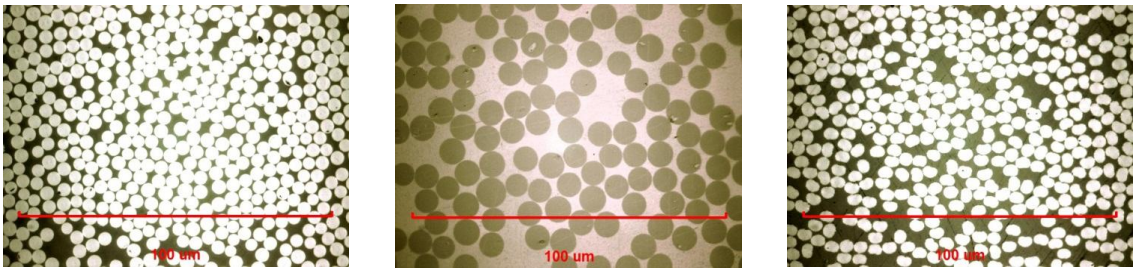

a) b) c)

Figure 4-8: Micrographs at x100 magnification: a) IM7/8552; b) S2/PMT-F7; c) M55J/RS-3.

Although the images in Figure 4-8 are a small sampling of the cross sectional surface in the laminates, an approximation can be made for fiber fraction in the lamina. The IM7/8552 laminate appears to be the densest with fiber. The M55/RS-3 laminate has more resin rich areas and general spacing between fibers. The S2/PMT-F7 lamina has the most resin rich areas compared with the other two and can be said to have the least fiber fraction of the three. The data analysis in the following three sections identifies the fiber volume fraction in the nonlinear cure fitting.

4.1 IM7/8552

Model fit results for all IM7/8552 samples are shown in Table 4-1, Figure 4-9, Figure 4-10, and Figure 4-11. The quality of the fit is not appreciably different between the different thicknesses but is great all around. The fits are exceptionally good for five ply and progressively worse as the thickness decreases. Figure 4-11 shows typical test data with model best fit curves and illustrates the lower fit quality of thinner coupons. Fiber volume fraction estimates had reasonable variation with thickness and proportionally increased with more plies as expected. The largest fiber volume average was in the four ply samples of 0.624 and the smallest was in the two ply of 0.590. The five ply laminates had the smallest variation in ply thickness of 0.9% but the thickest per ply average of 99.4 μm. The thinnest per ply average was in the four ply samples of 97.0 μm. All plies were in 2.0% thickness range within their appropriate ply set and in 2.5% range across the entire IM7/8552 sample set in which the final per ply average came out to be 98.2μm (Table 4-1).

The nonlinear parameter estimates were expected to be constant with thickness. Failing our expectations, the average for γ_C slowly increased with thickness as shown in Table 4-1. The variation is a likely effect of the tension fibers stabilizing the compression fibers and the effect changes with proximity between the two. The nonlinear parameter γ_C had an average of 20.7 across the entire IM7/8552 sample set. Murphey et al. calculated the compression parameter for IM7 fiber to be 29.6 from the compression data provided by Welsh et al. Due to a large variation in the modeled nonlinear parameter and its average not consistent with previously determined results we cannot support the recommendations set forth by Murphey et al. to use 29.6 as a nonlinear compression parameter for IM7 carbon composites.

Two of the twenty IM7/8552 data sets required an adjustment due to large variation of fitted parameters. The data was slightly truncated as discussed in section 3.10 to decrease variation and the statistical error of the nonlinear parameter. The root mean square statistics improved for the two modeled data sets and are apparent in the model fit quality plot. The root mean square value is subtracted from one in our table for ease of comparison.

The model indicates tensile fiber stiffening and compression softening at failure. The data table shows an average tensile modulus of 201 GPa for all plies and an average compressive modulus of 110 GPa for all plies. The results indicate a reasonable assumption for compressive modulus to be approximately two thirds of that determined from axial tensile tests by the manufacturer. Using the rule of mixtures we found an average compression modulus of the fiber to be 178.8 GPa. Fiber buckling load, which is of great concern in deployable structures, is less than the manufacturer specified.

The compressive strains modeled were largest in the thinner coupons and progressively got smaller with thickness while never reaching manufacturers reported strain of 1.8%. The average strain found was 1.68% for all plies tested. An example of modeled stress/strain curve with a linear model is shown in Figure 4-9. Same trend appeared in the tensile strains with the highest recorder average of 1.51%. The large compressive strains achieved in thinner samples are thought to be a result of structural stabilization. The proximity of fibers in tension to fibers in compression may be responsible for preventing those compressed fibers from microbuckling, a typical failure mode for fibers in compression, by increasing nearby stiffness.

All samples followed the same trend during failure as previously mentioned. In thicker samples partial delamination was observed between plies of the splintered pieces. All samples also exhibited signs of failure in form of subtle cracking moments prior to shattering and exploding across the laboratory test room.

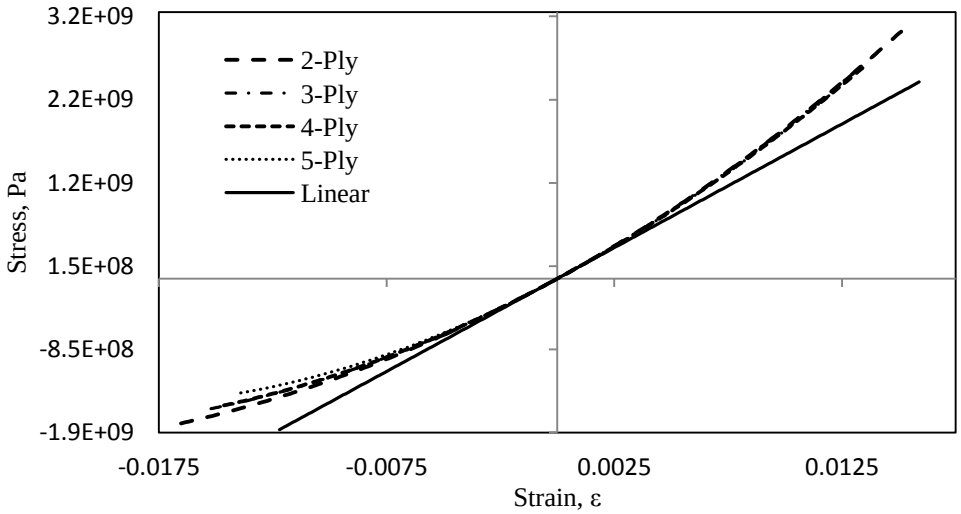

Figure 4-9: IM7/8552 composite constitutive behavior

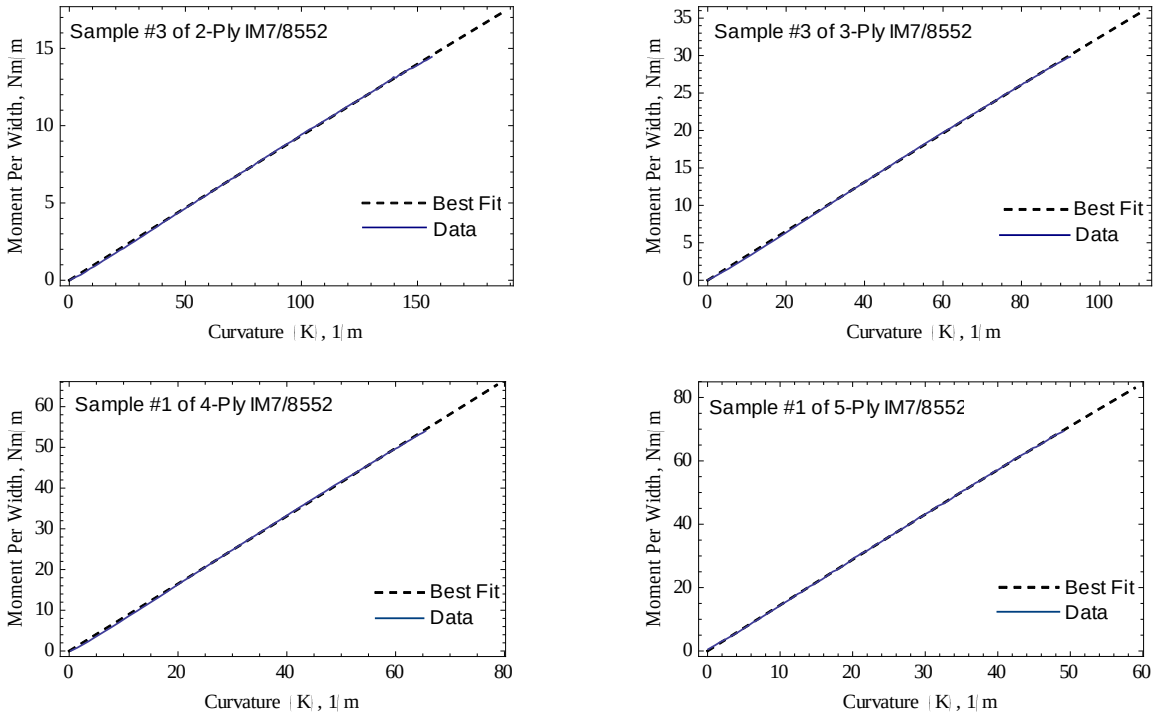

Figure 4-10: Typical fit results for IM7/8552

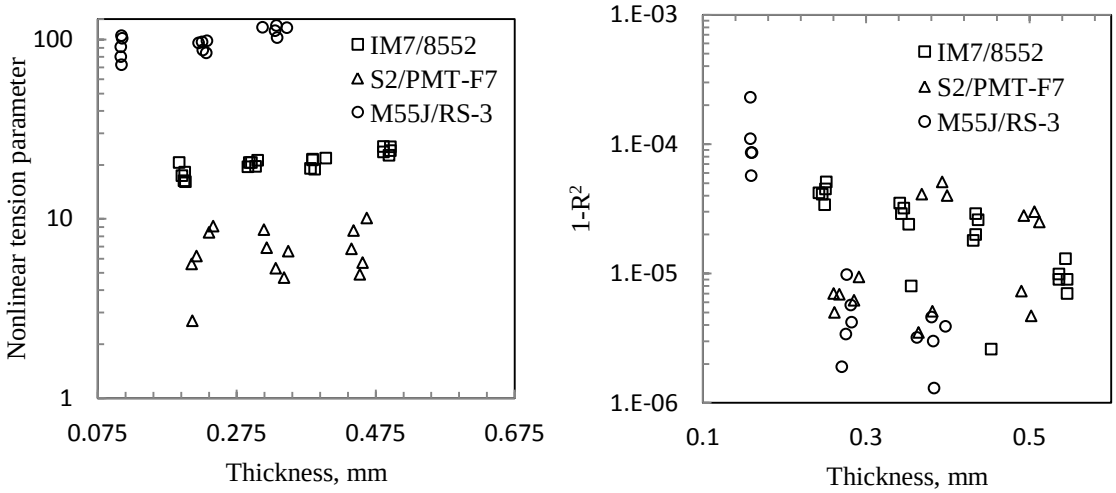

Figure 4-11: Model fit quality for IM7/8552, S2/PMT-F7, and M55J/RS-3

Table 4-1: Test results and model fit results for IM7/8552

Plies #	t mm	$\frac{y_{na}}{t}$	$\frac{M_f}{w}$ Nm/m	K_f m^{-1}	V_f	γ_C	1-R^2	$\varepsilon_{T,f}$	$\varepsilon_{C,f}$	$E_{T,f}$ GPa	$E_{C,f}$ GPa
2-02	0.199	0.023	27.0	147	0.610 ± 0.001	16.3 ± 0.8	3.4E-05	0.0140	0.0154	203.4	118.9
2-03	0.196	0.026	27.2	169	0.587 ± 0.001	17.4 ± 0.8	4.1E-05	0.0157	0.0175	202.3	107.9
2-06	0.200	0.026	27.9	163	0.579 ± 0.001	18.2 ± 0.8	4.5E-05	0.0155	0.0172	198.8	105.4
2-07	0.192	0.027	24.1	165	0.576 ± 0.001	20.6 ± 0.8	4.2E-05	0.0149	0.0167	196.2	101.1
2-08	0.201	0.025	29.8	163	0.600 ± 0.001	16.1 ± 0.9	5.1E-05	0.0156	0.0172	206.2	113.5
AVG	**0.198**	**0.025**	**27.2**	**161.4**	**0.590**	**17.7**	**4.26E-05**	**0.0151**	**0.0168**	**201.4**	**109.4**
STDV	**0.003**	**0.001**	**1.8**	**7.5**	**0.013**	**1.6**	**5.54E-06**	**0.001**	**0.001**	**3.5**	**6.2**
COV	**1.7%**	**5.3%**	**6.8%**	**4.7%**	**2.2%**	**9.2%**	**13.0%**	**4.2%**	**4.4%**	**1.7%**	**5.7%**
3-01	0.305	0.027	55.5	99	0.590 ± 0.000	21.2 ± 0.4	8.0E-06	0.0142	0.0158	198.2	104.3
3-02	0.302	0.025	57.0	98	0.613 ± 0.001	19.6 ± 0.7	2.4E-05	0.0140	0.0155	204.8	112.2
3-03	0.291	0.025	55.6	100	0.636 ± 0.001	19.5 ± 0.8	3.5E-05	0.0138	0.0153	211.3	117.1
3-04	0.296	0.026	52.5	101	0.603 ± 0.001	20.6 ± 0.8	3.2E-05	0.0141	0.016	202.2	108.2
3-05	0.293	0.027	51.4	105	0.582 ± 0.001	20.6 ± 0.8	2.9E-05	0.0145	0.0161	196.6	103.6
AVG	**0.297**	**0.026**	**54.4**	**100.6**	**0.605**	**20.3**	**2.56E-05**	**0.0141**	**0.0157**	**202.6**	**109.1**
STDV	**0.005**	**0.001**	**2.1**	**2.4**	**0.019**	**0.7**	**9.52E-06**	**2.32E-04**	**3.01E-04**	**5.2**	**5.1**
COV	**1.8%**	**3.4%**	**3.9%**	**2.4%**	**3.1%**	**3.2%**	**37.2%**	**1.6%**	**1.9%**	**2.6%**	**4.6%**
4-01	0.403	0.020	93.8	71	0.625 ± 0.001	21.8 ± 1.1	2.6E-06	0.0135	0.0149	191.0	120.0
4-02	0.387	0.023	90.1	98	0.635 ± 0.001	18.9 ± 0.8	2.6E-05	0.0133	0.0146	208.8	119.9
4-03	0.384	0.025	98.8	100	0.658 ± 0.001	21.3 ± 0.8	2.9E-05	0.0133	0.0147	216.4	118.7
4-04	0.381	0.024	83.2	101	0.592 ± 0.001	19.1 ± 0.7	1.8E-05	0.0138	0.0152	196.9	110.5
4-05	0.384	0.025	82.7	105	0.610 ± 0.001	21.5 ± 0.7	2.0E-05	0.0133	0.0147	201.2	110.0
AVG	**0.388**	**0.023**	**89.7**	**95.0**	**0.624**	**20.5**	**1.91E-05**	**0.0134**	**0.0149**	**202.9**	**115.8**
STDV	**0.008**	**1.87E-03**	**6.2**	**12.2**	**0.022**	**1.25**	**9.16E-06**	**0.0002**	**0.0002**	**8.9**	**4.6**
COV	**2.0%**	**8.1%**	**6.9%**	**12.9%**	**3.6%**	**6.1%**	**47.9%**	**1.5%**	**1.5%**	**4.4%**	**3.9%**
5-01	0.496	0.025	128.2	51	0.639 ± 0.001	25.2 ± 0.5	7.0E-06	0.0121	0.0133	206.0	112.3
5-02	0.486	0.025	123.0	55	0.579 ± 0.001	23.6 ± 0.5	9.0E-06	0.0128	0.0142	189.6	102.5
5-03	0.494	0.024	125.9	54	0.582 ± 0.001	22.6 ± 0.6	1.3E-05	0.0127	0.0140	190.1	105.1
5-04	0.496	0.026	126.6	52	0.617 ± 0.001	24.0 ± 0.5	9.0E-06	0.0131	0.0146	202.9	106.9
5-05	0.486	0.025	120.1	53	0.605 ± 0.001	25.3 ± 0.5	9.9E-06	0.0123	0.0136	195.9	105.4
AVG	**0.492**	**0.025**	**124.8**	**53.0**	**0.604**	**24.1**	**9.58E-06**	**0.0126**	**0.0139**	**196.9**	**106.4**
STDV	**0.005**	**6.32E-04**	**2.9**	**1.4**	**0.022**	**1.02**	**1.96E-06**	**0.0004**	**0.0005**	**6.6**	**3.3**
COV	**0.9%**	**2.5%**	**2.3%**	**2.7%**	**3.7%**	**4.2%**	**20.4%**	**2.8%**	**3.3%**	**3.4%**	**3.1%**

4.2 S2/PMT-F7 Results

Model fit results are tabulated for the S2/PMT-F7 in Table 4-2 and model fit quality shown in Figure 4-11. Typical test data for the three S2/PMT-F7laminate sets is shown in Figure 4-12. A zero term was expected for the nonlinear parameter from the model fitted to the S2 composite data described in section 3.9 knowing the tensile behavior of the fiber is linear. The average fitted parameter across the complete set of plies was found to be 6.7 with small disparity across thickness.

Although the results for the S2/PMT-F7 present a small nonlinear tension parameter they do not provide enough to conclude a nonlinear behavior in the laminate. A small non zero term verifies the miss-functionality of the model fit by returning a nonzero answer nested away from boundary conditions with small root mean square values. A number of model fits had to be adjusted to model a smaller sample of data due to initial large error in the nonlinear parameter. Post adjustment, the error of the fit was an order of magnitude smaller than of the initial fully fitted data.

The decreased quality of the fit in the thinner samples due to noise in the data required us to adjust the size of the data plot in the model fit. The qualities of the fit to the adjusted data sets were exceptional and are shown in Figure 4-11 and can be compared in Figure 4-12. All of the two ply and two plots from each of the three and four ply data were adjusted. Prior to adjustment, the fit quality increased with thickness similar to the IM7/8552 fit quality data.

The variation in fiber volume fraction increased compared to the IM7/8552 data. A variation of up to 7.1% was observed in the three ply data but overall average for the 15 tested samples was around two percent. Despite variation of per ply thickness as high

as 5.7% in one of the ply sets, the overall per ply thickness average of 111.15μm is considered excellent.

No S2/PMT-F7 coupon shattered into pieces during testing as previously mentioned. Most failed on the compression side in the outer most ply right at the edge of the clamping plate. The coupon appeared to develop a tiny gash parallel and next to the clamping plate which grew quickly as the testing continued. For most the gash initiated at the edge and advanced inward as shown in Figure 4-1. All coupons were tested until the gash had developed. While model fitting the data the initiation of failure was taking into account and a small segment at the end of each data set was left off for all S2/PMT-F7 model fits a sampling of which can be seen bellow.

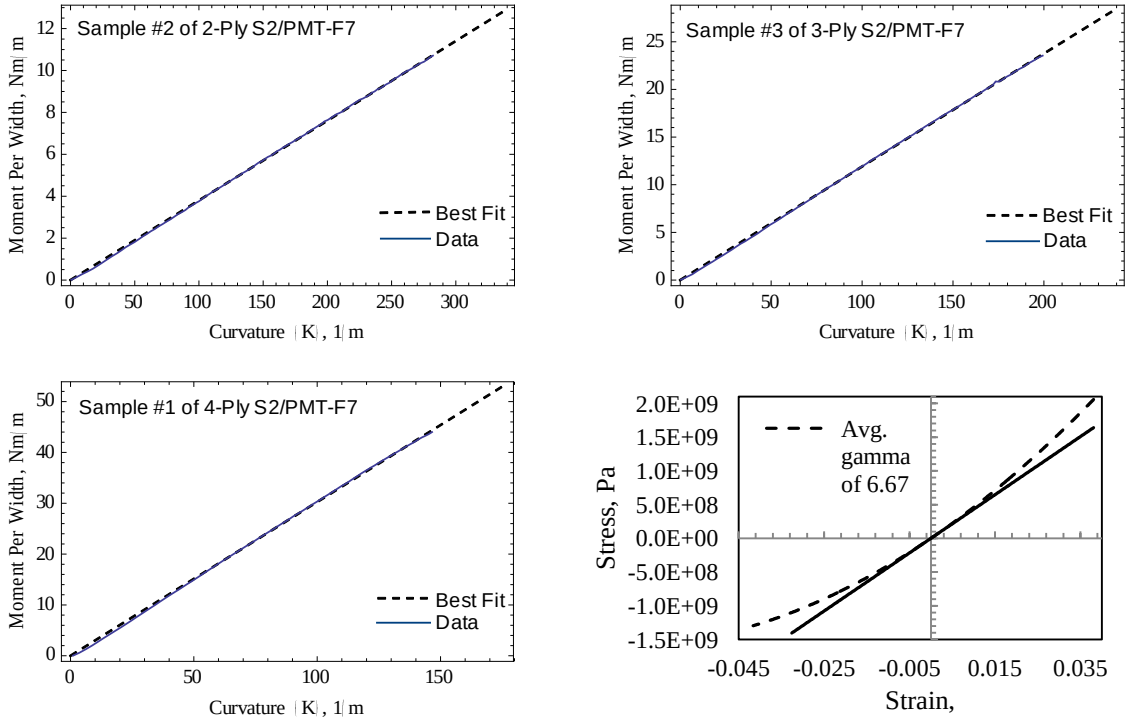

Figure 4-12: Typical fit results and model average axial constitutive behavior for S2/PMT-F7

Table 4-2: Test results and model fit results for S2/PMT-F7

Plies #	t mm	$\frac{y_{na}}{t}$	$\frac{M}{w}$ Nm/m	K_f m^{-1}	V_f	γ	$1-R^2$	$\varepsilon_{T,f}$	$\varepsilon_{C,f}$	$E_{T,f}$ GPa	$E_{C,f}$ GPa
2-01	0.211	0.008	22.3	368	0.474 ± 0.001	2.7 ± 2.1	5.0E-06	0.0358	0.0369	47.1	39.1
2-02	0.217	0.019	24.5	355	0.496 ± 0.001	6.2 ± 0.7	6.9E-06	0.0365	0.0394	55.4	35.1
2-04	0.210	0.016	24.2	413	0.473 ± 0.001	5.6 ± 0.7	7.0E-06	0.0341	0.0363	51.3	35.1
2-05	0.235	0.030	29.4	413	0.442 ± 0.000	8.4 ± 0.3	6.2E-06	0.0420	0.0474	55.8	26.5
2-06	0.241	0.033	29.7	414	0.433 ± 0.001	9.1 ± 0.3	9.4E-06	0.0420	0.0479	46.1	25.2
AVG	**0.223**	**0.021**	**26.0**	**393**	**0.464**	**6.4**	**6.90E-06**	**0.0381**	**0.0416**	**51.1**	**32.2**
STDV	**0.013**	**0.009**	**3.0**	**26**	**0.023**	**2.27**	**1.44E-06**	**0.0033**	**0.0051**	**4.0**	**5.4**
COV	**5.7%**	**43.4%**	**11.5%**	**6.6%**	**5.0%**	**35.4%**	**20.9%**	**8.7%**	**12.2%**	**7.9%**	**16.8%**
3-01	0.343	0.013	57.4	216	0.489 ± 0.001	4.7 ± 2.2	5.1E-05	0.0342	0.0360	51.4	37.4
3-02	0.331	0.017	54.4	241	0.464 ± 0.001	5.3 ± 0.8	5.1E-06	0.0361	0.0384	50.3	34.5
3-03	0.314	0.025	52.6	251	0.516 ± 0.000	8.7 ± 0.3	3.5E-06	0.0342	0.0379	61.3	33.2
3-04	0.318	0.021	56.1	252	0.524 ± 0.001	6.9 ± 1.1	4.1E-05	0.0358	0.0389	59.4	36.0
3-05	0.349	0.021	60.0	238	0.431 ± 0.001	6.6 ± 1.1	4.0E-05	0.0377	0.0409	51.1	31.2
AVG	**0.331**	**0.019**	**56.1**	**240**	**0.485**	**6.4**	**2.81E-05**	**0.0356**	**0.0384**	**54.7**	**34.5**
STDV	**0.014**	**0.004**	**2.5**	**13**	**0.034**	**1.39**	**1.98E-05**	**0.0013**	**0.0016**	**4.7**	**2.2**
COV	**4.1%**	**21.0%**	**4.5%**	**5.4%**	**7.1%**	**21.6%**	**70.5%**	**3.7%**	**4.1%**	**8.5%**	**6.3%**
4-01	0.440	0.022	85.1	188	0.471 ± 0.001	6.8 ± 0.7	7.3E-06	0.0379	0.0414	54.3	32.2
4-02	0.456	0.016	95.2	158	0.486 ± 0.001	5.7 ± 1.5	3.0E-05	0.0331	0.0353	52.5	36.2
4-03	0.443	0.024	90.7	171	0.471 ± 0.001	8.6 ± 0.8	2.8E-05	0.0337	0.0372	57.7	32.0
4-04	0.462	0.029	99.3	164	0.452 ± 0.001	10.1 ± 0.7	2.5E-05	0.0337	0.0379	58.2	28.7
4-06	0.452	0.013	98.5	163	0.496 ± 0.001	4.9 ± 0.8	4.7E-06	0.0330	0.0348	52.2	38.0
AVG	**0.451**	**0.021**	**93.8**	**169**	**0.475**	**7.2**	**1.90E-05**	**0.0343**	**0.0373**	**55.0**	**33.4**
STDV	**0.008**	**0.006**	**5.3**	**10**	**0.015**	**1.90**	**1.08E-05**	**0.0018**	**0.0023**	**2.5**	**3.3**
COV	**1.8%**	**27.4%**	**5.6%**	**6.2%**	**3.2%**	**26.3%**	**56.7%**	**5.3%**	**6.3%**	**4.6%**	**9.9%**

4.3 M55J/RS-3 Results

Large portion of the experimental data was adjusted by removing small initial section of data in order to improve the reliability of the model. The three ply laminate data had a lot of noise, shown in Figure 4-11, returning progressively worse fits even post adjustment. The fit quality is shown in Table 4-3. Fiber volume fraction estimates were consistent for

most part and there was reasonable variation with thickness. Ply thickness variation was reasonable for the 9 ply samples and improved in thinner samples.

Nonlinear parameters were expected to be constant with thickness and nonzero due to the nature of the fiber. As shown in Table 4-3, the nonlinear parameter is non-zero but does appear to have an increasing trend with thickness. The size of the nonlinear parameter does not simply correlate to the laminates nonlinear response but it is substantially larger than the nonlinear parameter of the IM7 carbon fiber. Looking at the constitutive plot shown in Figure 4-13 we can tell a definitive nonlinear behavior of the composite compared to its linear model.

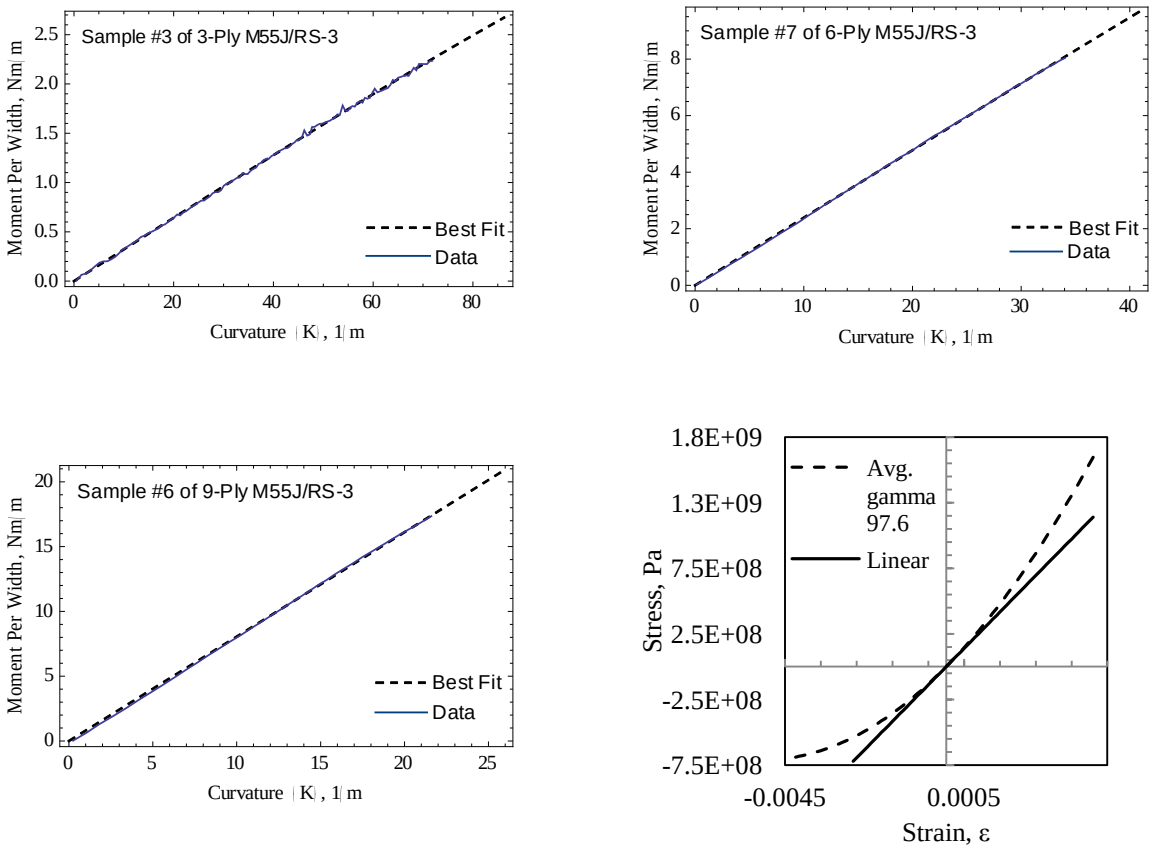

Figure 4-13: Typical fit results and model average axial constitutive behavior for M55J/RS-3

Table 4-3: Test results and model fit results for M55J/RS-3

Plies #	t mm	$\frac{y_{na}}{t}$	$\frac{M}{w}$ Nm/m	K_f m^{-1}	V_f	γ	$1-R^2$	$\varepsilon_{T,f}$	$\varepsilon_{T,f}$	$E_{T,f}$ GPa	$E_{C,f}$ GPa
3-03	0.110	0.036	4.4	77	0.541 ± 0.001	101.5 ± 7.0	8.6E-05	0.0039	0.0046	428.0	176.8
3-04	0.108	0.030	4.2	83	0.525 ± 0.002	80.2 ± 11.6	2.3E-04	0.0042	0.0048	392.7	188.7
3-06	0.109	0.040	4.4	87	0.601 ± 0.001	105.0 ± 4.6	5.7E-05	0.0042	0.0049	492.3	182.7
3-07	0.109	0.028	4.0	84	0.506 ± 0.001	72.3 ± 7.6	8.6E-05	0.0040	0.0050	369.7	189.3
3-08	0.108	0.036	4.1	87	0.523 ± 0.001	91.0 ± 6.5	1.1E-04	0.0044	0.0050	413.9	172.3
AVG	**0.109**	**0.033**	**4.2**	**84**	**0.539**	**86.8**	**1.02E-04**	**0.0041**	**0.0049**	**414.2**	**185.5**
STDV	**0.001**	**0.005**	**0.2**	**3.7**	**0.033**	**13.73**	**6.56E-05**	**0.0002**	**0.0001**	**43.4**	**5.1**
COV	**0.7%**	**14%**	**3.8%**	**4.4%**	**6.1%**	**15.8%**	**64.3%**	**4.2%**	**3.1%**	**10.5%**	**2.8%**
6-02	0.226	0.032	14.8	38	0.487 ± 0.001	87.3 ± 3.6	9.8E-06	0.0040	0.0046	369.0	171.7
6-03	0.232	0.035	16.2	37	0.510 ± 0.001	98.3 ± 3.1	4.2E-06	0.0040	0.0046	399.1	169.5
6-05	0.231	0.031	15.5	38	0.483 ± 0.001	84.2 ± 4.0	5.7E-06	0.0041	0.0046	363.3	172.3
6-06	0.225	0.035	14.8	38	0.498 ± 0.001	96.9 ± 3.7	3.4E-06	0.0040	0.0046	388.7	166.7
6-07	0.220	0.034	14.1	38	0.502 ± 0.001	95.7 ± 5.3	1.9E-06	0.0039	0.0045	389.2	170.2
AVG	**0.227**	**0.033**	**15.1**	**37.8**	**0.496**	**92.5**	**5.00E-06**	**0.0040**	**0.0046**	**381.9**	**170.1**
STDV	**0.004**	**0.002**	**0.7**	**0.4**	**0.010**	**5.64**	**2.70E-06**	**0.0001**	**0.0000**	**13.5**	**2.0**
COV	**1.9%**	**4.9%**	**4.7%**	**1.1%**	**2.0%**	**6.1%**	**53.9%**	**1.6%**	**0.9%**	**3.5%**	**1.2%**
9-01	0.333	0.035	33.8	25	0.493 ± 0.001	102.4 ± 6.2	1.3E-06	0.0038	0.0044	385.9	164.2
9-02	0.312	0.041	31.9	27	0.533 ± 0.001	116.9 ± 4.2	3.2E-06	0.0038	0.0045	440.8	159.8
9-05	0.347	0.043	37.4	25	0.484 ± 0.001	116.3 ± 5.1	3.9E-06	0.0040	0.0048	406.9	140.6
9-06	0.332	0.044	34.8	26	0.501 ± 0.001	119.6 ± 3.8	3.0E-06	0.0040	0.0048	424.0	143.1
9-07	0.330	0.042	34.2	26	0.502 ± 0.001	111.9 ± 5.8	4.6E-06	0.0039	0.0046	412.6	152.9
AVG	**0.331**	**0.041**	**34.4**	**25.8**	**0.503**	**113.4**	**3.20E-06**	**0.0039**	**0.0046**	**414.0**	**152.1**
STDV	**0.011**	**0.003**	**1.8**	**0.7**	**0.018**	**6.04**	**1.10E-06**	**0.0001**	**0.0002**	**18.2**	**9.2**
COV	**3.4%**	**7.7%**	**5.2%**	**2.9%**	**3.7%**	**5.3%**	**34.5%**	**2.3%**	**3.5%**	**4.4%**	**6.0%**

Chapter 5
Conclusion and Future Work

5.1 Conclusion

Three laminates were investigated for their use in deployable structures. Previously established nonlinear constitutive behavior in large flexures was investigated by means of fitting first degree models with nonlinear constitutive parameters to experimental EI data. The thesis is motivated by the need for an accurate nonlinear elastic constitutive model for carbon fiber composites.

Carbon fiber composites have generated significant interest for use in areas where high stiffness yet flexible materials can replace traditional mechanisms. Thin composite flexures may replace heavier, less reliable and costly hinge type devices. Experimental investigation of flexural behavior using a newly designed bending fixture in which pure moment is applied to the gage section was reported for laminates made of IM7/8552, S2/PMT-F7, and M55J/RS-3.

The description of the test device, which measured the combined effect of lamina tensile and compression behavior, as well as testing protocol are described in detail. For validation of the test device well-documented spring steel samples were tested and reported on. Potential source for error is identified and its presence is used to adjust some of the data for modeling in order to decrease statistical error. The fixture provided a clean and reliable data of the investigated materials in the test campaign which was noted from the consistency of the material failure at the same curvature with respect to thickness.

The test coupons failed along the edge of the grips and not the middle of the gage section as intended. Stress concentration along the edge was observed in S2 test specimens in which the compression side of the material began to shear across at the contact edge with the grip. Failure at the grips suggests the test fixture should not be used to find true strength of the material. It is great for large strain testing of thin laminates and can be used to find appropriate nonlinear constitutive parameters to accurately represent the materials' nonlinear behavior.

A process to manufacture geometrically consistent laminates from the materials of interest is reported in detail above and is the key for accurate measurements using the test fixture. Much needed micrographing procedure, used to accurately record the thickness of tested laminates, is also discussed. The empirical models, which rely on accurate laminate thickness report, measured load, displacement quantities, and their calculations are explained. Distinction between models used to fit data with two different nonlinear parameters, one in tension and one in compression, and one parameter for both tension and compression, is identified.

Prior estimate for nonlinear constitutive parameter in tension, of 21.4, was used in IM7/8552 model fit to find an accurate estimate for nonlinear constitutive parameter in compression. The found average nonlinear constitutive parameter in compression of 20.7 is significantly lower than previously reported compression parameter of 29.6 [31]. The nonlinear compression parameter for the two ply laminates was lower than our calculated average but increased with thickness.

No previous estimates have been made for nonlinear model parameters of M55J and no signs of nonlinear behavior have been observed for S2 in prior testing and were not expected here. A constitutive model with same nonlinear parameter for tension and compression was used to fit the flexural data from S2/PMT-F7 and M55J/RS-3. Due to the fact that we know S2 behavior to be linear in tension and our nonlinear curve fitting returned an average nonlinear constitutive parameter of 6.67, we conclude that this model cannot be used to find both parameters. The curve fitting average nonlinear constitutive parameter for M55J was found to be 97.6, but due to the problem with the model, the determined fit parameter cannot be used reliably until further investigation.

We provided experimental evidence that demonstrated the ability of the fixture to produce data that can be used to calculate the moment vs. curvature response of material in question. The moment vs. curvature response of the laminates which characterize flexural behavior was accurately fitted with a first order empirical strain and stress based model for IM7 carbon fiber. The model used to find nonlinear parameters for M55J and S2 is inaccurate. Moreover, the nonlinear tensile behavior appears to counteract nonlinear compressive behavior to give a fairly linear behavior as observed from the moment vs. curvature response plots of the data collected.

5.1 Future Work

There are still many nuances of modeling composite materials we have not considered starting with laminate testing and ending with and FEA analysis using nonlinear modeled behavior. First, the boundary conditions of the test fixture need to be closely examined and preferably solved so the fixture can also be used to properly measure material strength in addition to strain. Also, the fixture did not always translate towards the center requiring the operator to lightly adjust the carts introducing parasitic load. This problem can possibly be solved with a self-centering mechanism.

The model established in this thesis for IM7 is only applicable to the fiber direction property of the hyper-elastic material. To properly model transversely-isotropic material in FEA, the material properties normal to fiber direction are necessary. Currently we do not have the data to accurately model material properties normal to the fiber direction. Figuring out those materials properties would be a good step towards accurately using FEA in design and development of structures made of thin carbon fiber laminates.

The model used to fit for nonlinear constitutive parameters of S2 and M55J was found unreliable. Knowing the S2 tensile behavior to be linear we can use the same model we used for IM7 and set the nonlinear constitutive tensile parameter to zero. Tensile data for M55J is needed so a nonlinear tension parameter can be estimated first, and then used to fit for the compressive nonlinear parameter.

A possible way to obtain such data is to use laminates made of half fiber and half know material with linear constitutive behavior for testing in the test fixture. Tensile and compressive parameter can be found using such a laminate while accounting for the

known material behavior and shift of the neutral axis. Other materials with even higher strain to failure than IM7 are now available on the market. They are of interest for use in the deployable structures and can be implemented into a future test campaign.

References

[1] J. M. Mejia-Ariza, T. W. Murphey, and H.-P. Dumm, "Deployable Trusses Based on Large Rotation Flexure Hinges," *Journal of Spacecraft and Rockets*, vol. 47, no. 6, pp. 1053-1062, 2010.

[2] T. W. Murphey, S. Jeon, A. Biskner, and G. Sanford, "Deployable Booms and Antennas Using Bi-stable Tape-springs," in *24th Annual AIAAUSU Conference on Small Satellites*, 2010, no. 505, p. SSC10-X-6.

[3] G. J. Curtis, J. M. Milne, and W. N. Reynolds, "Non-Hookean behaviour of Strong Carbon Fibres," *Nature*, vol. 220, no. 7, pp. 1024-1025, 1968.

[4] W. Reynolds and J. Sharp, "Crystal shear limit to carbon fibre strength," *Carbon*, vol. 12, no. 2, pp. 103–110, 1974.

[5] L. Fischer and W. Ruland, "The influence of graphitization on the mechanical properties of carbon fibers," *Colloid and Polymer Science*, vol. 258, no. 8, pp. 917-922, 1980.

[6] M. Guigon, A. Oberlin, and G. Desarmot, "Microtexture and structure of some high tensile strength, PAN-base carbon fibres," *Fibre Science And Technology*, vol. 20, no. 1, pp. 55-72, 1984.

[7] M. Northolt and R. Hout, "Elastic extension of an oriented crystalline fibre," *Polymer*, vol. 26, no. 2, pp. 310–316, 1985.

[8] S. C. Bennett, D. L. Johnson, and W. Johnson, "Strength-structure relationships in PAN-based carbon fibres," *Journal of Materials Science*, vol. 18, no. 11, p. 3337, 1983.

[9] D. Loidl, O. Paris, M. Burghammer, C. Riekel, and H. Peterlik, "Direct observation of nanocrystallite buckling in carbon fibers under bending load.," *Physical Review Letters*, vol. 95, no. 22, p. 225501, 2005.

[10] W. R. Jones and J. W. Johnson, "Intrinsic strength and non-hookean behaviour of carbon fibres," *Carbon*, vol. 9, no. 5, pp. 645-655, 1971.

[11] N. Melanitis and C. Galiotis, "Compressional behaviour of carbon fibres," *Journal of Materials Science*, vol. 25, no. 12, pp. 5081-5090, 1990.

[12] N. Oya and D. J. Johnson, "Longitudinal compressive behaviour and microstructure of PAN-based carbon fibres," *Carbon*, vol. 39, no. 5, pp. 635-645, 2001.

[13] M. R. Wisnom, J. W. Atkinson, and M. I. Jones, "Reduction in compressive strain to failure with increasing specimen size in pin-ended buckling tests," *Composites Science and Technology*, vol. 57, no. 9-10, pp. 1303-1308, 1997.

[14] J. M. Whitney and M. Knight, “The relationship between tensile strength and flexure strength in fiber-reinforced composites,” *Experimental Mechanics*, vol. 20, no. 6, pp. 211-216, 1980.

[15] D. Sinclair, “A Bending Method for Measurement of the Tensile Strength and Young’s Modulus of Glass Fibers,” *Journal of Applied Physics*, vol. 21, no. 5, p. 380, 1950.

[16] D. Thorne, “Carbon fibres with large breaking strain,” *Nature*, vol. 248, no. 26, pp. 754-756, 1974.

[17] M. R. Wisnom, “On the high compressive strains achieved in bending tests on unidirectional carbon-fibre/epoxy,” *Composites Science and Technology*, vol. 43, no. 3, pp. 229-235, 1992.

[18] S. Jeon and T. W. Murphey, “Design and analysis of a meter-class CubeSat boom with a motor-less deployment by bi-stable tape springs,” in *52nd AIAAASMEASCEAHSASC Structures Structural Dynamics and Materials Conference*, 2011, no. April.

[19] J. A. Banik and T. W. Murphey, “Performance Validation of the Triangular Rollable and Collapsible Mast,” in *24th Annual AIAAUSU Conference on Small Satellites*, 2010, p. SSC10-II-1.

[20] F. A. Roybal, J. A. Banik, and T. W. Murphey, “Development of an Elastically Deployable Boom for Tensioned Planar Structures,” in *48th AIAAASMEASCEAHSASC Structures Structural Dynamics and Materials Conference*, 2007, no. April, pp. AIAA 2007-1838.

[21] G. E. Sanford, E. V. Ardelean, T. W. Murphey, and M. M. Grigoriev, “HIGH STRAIN TEST METHOD FOR THIN COMPOSITE LAMINATES.” ICCS 16, p. 13, 2011.

[22] “ASTM D3039 Standard Test Method for Tensile Properties of Polymer Matrix Composite Materials 1,” *Transition*, vol. i, pp. 1-13, 2008.

[23] ASTM D 6272, “Standard Test Method for Flexural Properties of Unreinforced and Reinforced Plastics and Electrical Insulating Materials by Four-Point Bending 1,” vol. 8, no. June, pp. 1-11, 2002.

[24] R. M. Jones, “Apparent flexural modulus and strength of multimodulus materials,” *Journal of Composite Materials*, vol. 10, no. 4, pp. 342-354, 1976.

[25] T. K. O’Brien, A. D. Chawan, K. Demarco, and I. Paris, “Influence of Specimen Preparation and Specimen Size on Composite Transverse Tensile Strength and Scatter,” *TM NASA STI*, no. July, 2001.

[26] T. K. O’Brien, A. D. Chawan, and R. Krueger, “Characterization Through Flexure Testing of Composite Materials,” *TM NASA STI*, no. July, 2001.

[27] F. Mujika, “On the difference between flexural moduli obtained by three-point and four-point bending tests,” *Polymer Testing*, vol. 25, no. 2, pp. 214-220, 2006.

[28] M. Hyer, *Stress Analysis of Fiber-Reinforced Composite Materials*, Updated Ed. DEStech Publications, Inc., 2009.

[29] T. Ishikawa, M. Matsushima, and Y. Hayashi, “Hardening nonlinear behaviour in longitudinal tension of unidirectional carbon composites,” *Journal of Materials Science*, vol. 20, no. 11, pp. 4075-4083, 1985.

[30] C. Reder et al., “Non-contacting strain measurements of ceramic and carbon single fibres by using the laser-speckle method,” *Composites Part A Applied Science and Manufacturing*, vol. 34, no. 11, pp. 1029-1033, 2003.

[31] T. W. Murphey, G. E. Sanford, and M. M. Grigoriev, “NONLINEAR ELASTIC CONSTITUTIVE MODELING OF LARGE STRAINS IN CARBON FIBER COMPOSITE FLEXURES,” 2011.

[32] J. Hughes, “Strength and modulus of current carbon fibres,” *Carbon*, vol. 24, no. 5, pp. 551-556, 1986.

[33] W. H. M. Van Dreumel and J. L. M. Kamp, “Non Hookean behaviour in the fibre direction of carbon-fibre composites and the influence of fibre waviness on the tensile properties,” *Journal of Composite Materials*, vol. 11, no. 4, pp. 461-469, 1977.

[34] J. S. Welsh, J. S. Mayes, and A. C. Biskner, “EXPERIMENTAL AND NUMERICAL FAILURE PREDICTIONS OF BIAXIALLY-LOADED QUASI-ISOTROPIC CARBON COMPOSITES,” *Carbon*, pp. 1-10, 2007.

[35] R. Bullock, “Strength ratios of composite materials in flexure and in tension,” *Journal of Composite Materials*, vol. 8, pp. 200–206, 1974.

[36] G. Sanford, A. Biskner, and T. W. Murphey, “Large Strain Behavior of Thin Unidirectional Composite Flexures,” in *51st AIAAASMEASCEAHSASC Structures Structural Dynamics and Materials Conference*, 2010, pp. AIAA-2010-2698.

[37] “Nachi Fujikoshi Corp.” [Online]. Available: www.nachi.de.

[38] R. S. Figliola and D. E. Beasley, *Theory and Design for Mechanical Measurements*, 3rd ed. John Wiley& Sons, Inc., 2000, pp. 121-123.

[39] L. P. Marks and A. P. Marks, *Marks’ Standard Handbook for Mechanical Engineers*, 8th ed. McGraw-Hill, Inc., 1978, pp. 3-38.

[40] K. J. Åström, “Friction Models and Friction Compensation,” *Control*, vol. 4, no. 3, pp. 1-37, 1998.

Appendix A

VISION • VALUE • INTEGRITY

Certificate of Calibration

Report Number:
2780407

Department:
527 EMXS / MXDC
5909 Southgate Ave., Bldg. 214
Hill AFB, UT 84056

Date of Calibration:
28-Apr-11

Calibration Item

Manufacturer:	MILSP
Model/Part No.:	81
Equipment Type:	Gage Block Set, Working
Serial Number:	81507.1
ID Number:	J146399
Material:	Steel

Equipment Submitted By:
377 MXG / MXP
3500 RANDOLF AVE SE / BLDG 325 W
KIRTLAND AFB, NM 87117-5722

Room Ambient Conditions:
Temperature: 67.9º F Relative Humidity: 33%

Remarks:
Due to nicks and burrs on the gaging surfaces, the gage blocks were deburred prior to calibration.
Rust and burrs on the non-gaging surfaces do not affect measurement accuracy.
The gage blocks meet the limited T.O. specifications.
The T.O. directed limitation indicates the gage blocks are not calibrated to the manufacturer's specifications.

Traceability:

Measurement standards and test equipment used are traceable to the National Institute of Standards and Technology.

PROCEDURES

Title:	T.O. Number	T.O. Date
Calibration Procedure for Gage Blocks	33K6-4-1-1	30-Jun-10

EQUIPMENT

Nomenclature	ID#	Date Due Cal
Interferometer	G094329	20120421
Gage Block Comparator	F107672	20110602
Gage Block Set	G151096	20111028

Calibrated by:
Shelly Southwick
Calibration Technician

Approved By:
Gary Quigley
Physical/Dimensional Laboratory Lead

Report Number: 2780407
Date of Calibration: 28-Apr-11
Model/Part No.: 81
Serial Number: 81507.1
ID Number: J146399

Reported Values and Measurement Uncertainty:

Reported Values: The deviations in length from the nominal gage block sizes at 68°F are reported in the Gage Block Calibration Data Table that follows.

The reported deviations from nominal have a measurement accuracy of ±20 µin from stated deviation.

Deviation from nominal length is reported in µin. A minus sign (-) indicates the gage block is shorter than the nominal length. No sign indicates a plus (+) value and that the gage block is longer than the nominal length.

GAGE BLOCK CALIBRATION DATA TABLE

Nominal Size (In)	S/N	DEV(µin)	Nominal Size (In)	S/N	DEV(µin)	Nominal Size (In)	S/N	DEV(µin)
0.050	VCJ002	-2	0.117	VCJ002	0	0.144	VCJ002	-2
0.100	VCJ002	-1	0.118	070798	2	0.145	VCJ002	0
0.1001	VCJ002	-1	0.119	VCJ002	-3	0.146	VCJ002	-3
0.1002	VCJ002	0	0.120	VCJ002	-3	0.147	VCJ002	-5
0.1003	VCJ002	0	0.121	VCJ002	0	0.148	VCJ002	-1
0.1004	VCJ002	-1	0.122	VCJ002	-1	0.149	VCJ002	0
0.1005	VCJ002	-2	0.123	VCJ002	-1	0.150	VCJ002	-1
0.1006	Y5J041	-2	0.124	VCJ002	-5	0.200	VCJ002	-4
0.1007	VCJ002	0	0.125	VCJ002	1	0.250	VCJ002	3
0.1008	VCJ002	0	0.126	VCJ002	-1	0.300	VCJ002	0
0.1009	VCJ002	-1	0.127	VCJ002	1	0.350	VCJ002	-1
0.101	VCJ002	-3	0.128	VCJ002	-1	0.400	VCJ002	2
0.102	VCJ002	-2	0.129	VCJ002	-1	0.450	VCJ002	-3
0.103	VCJ002	-4	0.130	VCJ002	0	0.500	VCJ002	2
0.104	VCJ002	-2	0.131	VCJ002	0	0.550	VCJ002	-1
0.105	VCJ002	-3	0.132	VCJ002	-1	0.600	VCJ002	3
0.106	VCJ002	1	0.133	VCJ002	0	0.650	VCJ002	-3
0.107	VCJ002	-3	0.134	VCJ002	-3	0.700	VCJ002	7
0.108	VCJ002	-3	0.135	VCJ002	1	0.750	VCJ002	2
0.109	VCJ002	-3	0.136	VCJ002	0	0.800	VCJ002	4
0.110	VCJ002	-1	0.137	VCJ002	-2	0.850	VCJ002	2
0.111	VCJ002	-1	0.138	VCJ002	-4	0.900	VCJ002	9
0.112	VCJ002	0	0.139	VCJ002	-3	0.950	VCJ002	3
0.113	VCJ002	0	0.140	VCJ002	-5	1.000	VCJ002	-2
0.114	VCJ002	-2	0.141	VCJ002	-1	2.000	VCJ002	0
0.115	VCJ002	-4	0.142	VCJ002	-3	3.000	VCJ002	2
0.116	VCJ002	-3	0.143	VCJ002	-2	4.000	VCJ002	1

No accessories with set

Prüfbericht / Test Report

optoNCDT

MICRO-EPSILON

Modell	Model	*1700-100.000*
Serien-Nr.	Serial-No.	*0806017*
Meßbereich	Measuring Range in [mm]	*100*
Datum	date	*2008-06-06*

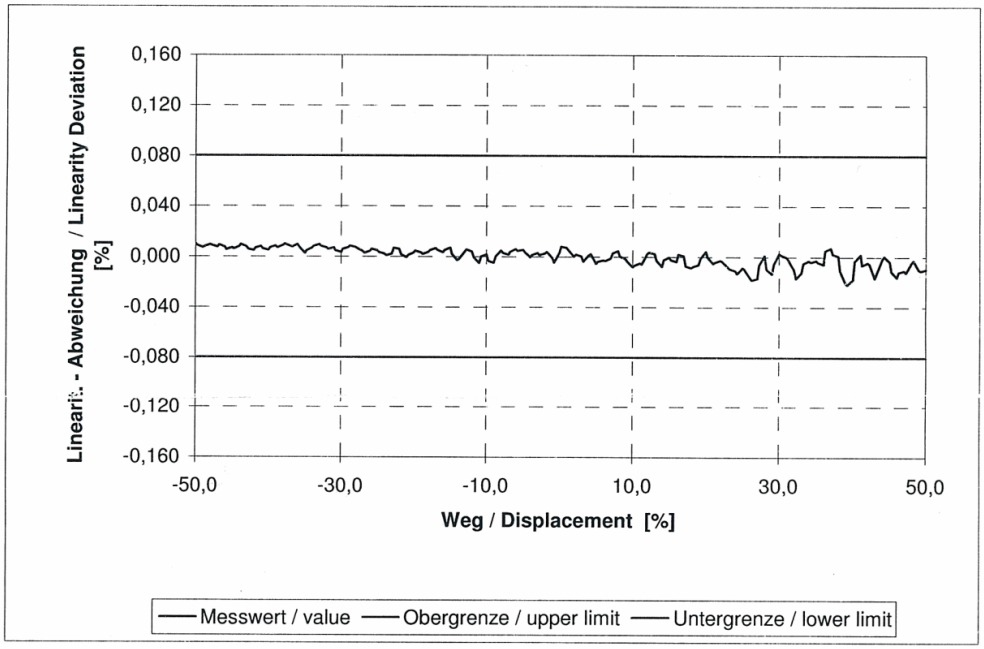

Dieser Prüfbericht gilt für die angegebene Systemzusammenstellung.
Messobjekt für den Test: Keramik weiss und eben
Die ermittelte Kennlinie ist als Werkskalibrierung im System hinterlegt.
Abweichungen von diesen Daten können auftreten durch:
- Rauigkeit der Oberfläche
- Sensormontage (Verkippung)
- Temperaturschwankungen während der Messung
- Zirkulation warmer Luft zwischen Sensor und Meßobjekt
- abweichende Reflexionseigenschaften der Oberfläche

Für weitere Informationen beachten Sie bitte
die Hinweise in der Bedienungsanleitung

This Test Report is valid for the reported system configuration
Target: withe ceramic (flat)
The above characteristics is stored as factory calibration.
Differences of these data can appear because of
-roughness of surface
-sensor mounting (tilt)
-fluctuations of temperature during the measurement
-circulation of hot air between sensor and target
-deviation of reflection attribute of surface

Further the statements in the operating manual are valid

Micro - Epsilon - Optronic GmbH / Lessingstraße 14 / D - 01465 Dresden - Langebrück
Tel.: +49 / 35201 / 729 - 0; Fax: +49 / 35201 / 729 - 90; e-mail: optronic@micro-epsilon.de; http://www.micro-epsilon.com

Prüfbericht / Test Report

optoNCDT

MICRO-EPSILON

Modell	Model	*1700-100.000*
Serien-Nr.	Serial-No.	*0712072*
Meßbereich	Measuring Range in [mm]	*100*
Datum	date	*2008-01-04*

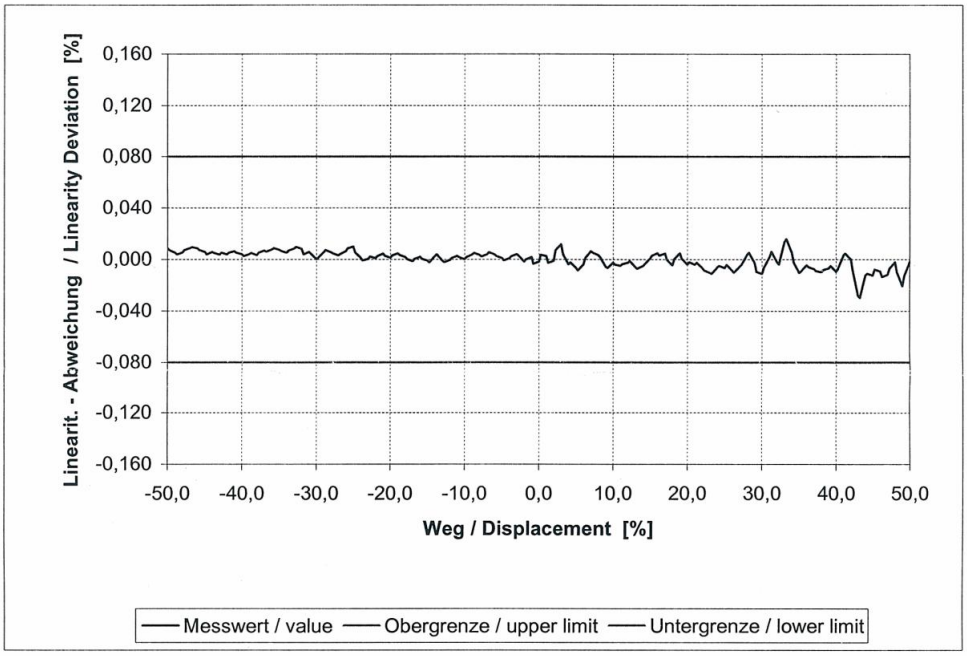

Dieser Prüfbericht gilt für die angegebene Systemzusammenstellung.
Messobjekt für den Test: Keramik weiss und eben
Die ermittelte Kennlinie ist als Werkskalibrierung im System hinterlegt.
Abweichungen von diesen Daten können auftreten durch:
- Rauigkeit der Oberfläche
- Sensormontage (Verkippung)
- Temperaturschwankungen während der Messung
- Zirkulation warmer Luft zwischen Sensor und Meßobjekt
- abweichende Reflexionseigenschaften der Oberfläche

Für weitere Informationen beachten Sie bitte
die Hinweise in der Bedienungsanleitung

This Test Report is valid for the reported system configuration
Target: withe ceramic (flat)
The above characteristics is stored as factory calibration.
Differences of these data can appear because of
-roughness of surface
-sensor mounting (tilt)
-fluctuations of temperature during the measurement
-circulation of hot air between sensor and target
-deviation of reflection attribute of surface
Further the statements in the operating manual are valid

Micro - Epsilon - Optronic GmbH / Lessingstraße 14 / D - 01465 Dresden - Langebrück
Tel.: +49 / 35201 / 729 - 0; Fax: +49 / 35201 / 729 - 90; e-mail: optronic@micro-epsilon.de; http://www.micro-epsilon.com

Calibration Details for JCN #: 201011221717

UUT Label Number: F176981
Serial #: 6981
Cal TO: 33K6-4-2949-1 **Cal Authority:** K100
OWC: M9044 **Organization:** AFRL

Part Number: PRO360
Nomenclature: CLINOMETER, ELECTRONIC
Off Sym: RVSV
Date Last Cal: 09-DEC-2010
Date Due Cal: 09-MAR-2012

Job Control Number: 201011221717

Type Maint:	Act Tkn:	When Disc:	How Mal:
J	J	T	799

Cert Tech: G11/5 MCMILLAN, DAVID
Cert TO: 33K6-4-2949-1
Cert Date Last Cal: 09-DEC-2010
Cert Cal Int: 15
JCN Remarks:

Temperature: 73.4 **% Humidity:** 35
Condition Received: A - In-Tolerance
Condition Returned: G - In-Tolerance

Corrective Action: Cal Complete. S/N: 6981

Special: S/N: 6981

Standards Used to Calibrate the Unit Under Test on this Job: 3

Label # / Nomenclature	Part #	OWC	Serial # / Cal Source	Cal TO	Cal Int	Date Due Cal / Date Used
A119036	GGG-P-463		415367		24	06-MAY-2013
SURFACE PLATE, GRANITE		M4500	K100	N47		09-DEC-2010
A133987	960-613		454		12	19-MAY-2012
LEVEL, PRECISION		M4500	K100	33K6-4-54-1		09-DEC-2010
E218514	CD12MCDLV-1		512101-31		60	27-JAN-2014
INDEXING TABLE		M4500	K100	AFPSL T.O.		09-DEC-2010

Force Calibration Report
20110210-KMR-000026-02

Serial Number: **305031**
Manufacturer: MTS Systems
Model Number: 4501027
System Name: SINTECH 1
Customer Name: AFRL, Kirtland AFB. NM
Calibration Date: February 07, 2011
Calibration By: Kraig Rowe
Cable Length: 24 inches
Environment: 75.5 °F, 21.6 %RH
FullScale: 225.00 lbf

Resolution 0.01, measured at 10 lbf
Calibration Range ±11.25 to 225.00 lbf

Rotation Position, Run 1 - 0 Degrees, Run 2 - 120 Degrees, Run 3 - 240 Degrees

Manual Entry Information
Manufacturer: MTS Systems
Controller: 21332
Model Number: TestWorks 4.11C
Serial Number: 967
Hardware Chan: _Load

5 to 100 Percent
As Found, Run 1

	Compression				
	Target	Standard	UUT	Error	%
Initial Zero	0.00	0.02	-0.02	-0.04	n/a
-5.0%	-11.25	-10.68	-10.65	0.03	0.28
-10.0%	-22.50	-22.87	-22.84	0.03	0.13
-20.0%	-45.00	-47.99	-47.99	0.00	0.00
-30.0%	-67.50	-69.10	-69.12	-0.02	-0.03
-40.0%	-90.00	-93.72	-93.73	-0.01	-0.01
-50.0%	-112.50	-113.81	-113.84	-0.03	-0.03
-60.0%	-135.00	-139.97	-140.03	-0.06	-0.04
-70.0%	-157.50	-159.35	-159.37	-0.02	-0.01
-80.0%	-180.00	-185.40	-185.46	-0.06	-0.03
-90.0%	-202.50	-205.30	-205.36	-0.06	-0.03
-100.0%	-225.00	-229.80	-229.85	-0.05	-0.02
Return to Zero	0.00	-0.06	0.00	0.06	n/a

	Tension				
	Target	Standard	UUT	Error	%
Initial Zero	0.00	0.00	0.00	0.00	n/a
5.0%	11.25	10.37	10.36	-0.01	-0.10
10.0%	22.50	22.49	22.48	-0.01	-0.04
20.0%	45.00	45.94	46.03	0.09	0.20
30.0%	67.50	69.04	69.05	0.01	0.01
40.0%	90.00	90.59	90.61	0.02	0.02
50.0%	112.50	111.90	111.90	0.00	0.00
60.0%	135.00	137.77	137.90	0.13	0.09
70.0%	157.50	158.27	158.41	0.14	0.09
80.0%	180.00	182.22	182.40	0.18	0.10
90.0%	202.50	204.80	205.03	0.23	0.11
100.0%	225.00	226.53	226.82	0.29	0.13
Return to Zero	0.00	-0.35	-0.37	-0.02	n/a

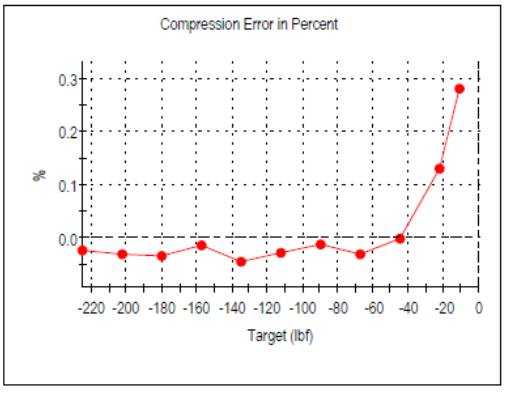

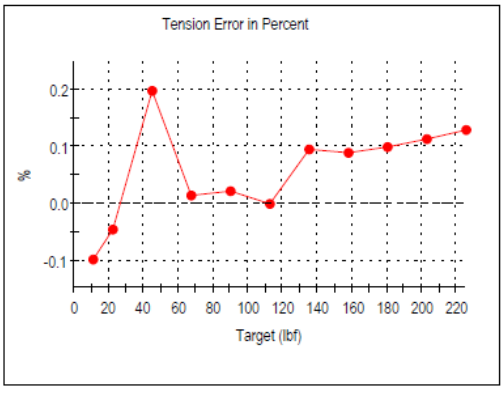

Force Calibration Report
20110210-KMR-000023-02

Serial Number: **E42209**
Manufacturer: MTS Systems
Model Number: 4501008/B
System Name: QTest 1L
Customer Name: AFRL, Kirtland AFB. NM
Calibration Date: February 09, 2011
Calibration By: Kraig Rowe
Cable Length: 24 inches
Geo Factor: 0.9985
Environment: 73.7 °F, 17.5 %RH
FullScale: 20.000 lbf

Resolution 0.003, measured at 1 lbf
Calibration Range ±1.000 to 20.000 lbf

Rotation Position - Run 1 - 0 Degrees, Run 2 - 120 Degrees, Run 3 - 240 Degrees.

Manual Entry Information
Manufacturer: MTS Systems
Controller: 21332
Model Number: TestWorks 4.11C
Serial Number: 967
Hardware Chan: _Load

20 lbf Dead Weight Schedule
As Found, Run 2

	Compression				
	Target	Standard	UUT	Error	%
Initial Zero	0.000	0.000	0.000	0.000	n/a
-1 lbf weight	-1.000	-0.999	-1.000	-0.001	-0.10
-2 lbf weight	-2.000	-1.997	-2.000	-0.003	-0.15
-4 lbf weight	-4.000	-3.994	-4.000	-0.006	-0.15
-6 lbf weight	-6.000	-5.991	-6.000	-0.009	-0.15
-8 lbf weight	-8.000	-7.988	-8.000	-0.012	-0.15
-10 lbf weight	-10.000	-9.985	-9.995	-0.010	-0.10
-12 lbf weight	-12.000	-11.982	-12.000	-0.018	-0.15
-14 lbf weight	-14.000	-13.979	-14.000	-0.021	-0.15
-16 lbf weight	-16.000	-15.976	-16.010	-0.034	-0.21
-18 lbf weight	-18.000	-17.973	-18.010	-0.037	-0.21
-20 lbf weight	-20.000	-19.970	-20.030	-0.060	-0.30
Return to Zero	0.000	0.000	0.000	0.000	n/a

	Tension				
	Target	Standard	UUT	Error	%
Initial Zero	0.000	0.000	0.000	0.000	n/a
1 lbf weight	1.000	0.999	1.000	0.001	0.10
2 lbf weight	2.000	1.997	2.000	0.003	0.15
4 lbf weight	4.000	3.994	4.000	0.006	0.15
6 lbf weight	6.000	5.991	5.990	-0.001	-0.02
8 lbf weight	8.000	7.988	8.000	0.012	0.15
10 lbf weight	10.000	9.985	10.010	0.025	0.25
12 lbf weight	12.000	11.982	12.020	0.038	0.32
14 lbf weight	14.000	13.979	14.020	0.041	0.29
16 lbf weight	16.000	15.976	16.020	0.044	0.28
18 lbf weight	18.000	17.973	18.020	0.047	0.26
20 lbf weight	20.000	19.970	20.030	0.060	0.30
Return to Zero	0.000	0.000	0.000	0.000	n/a